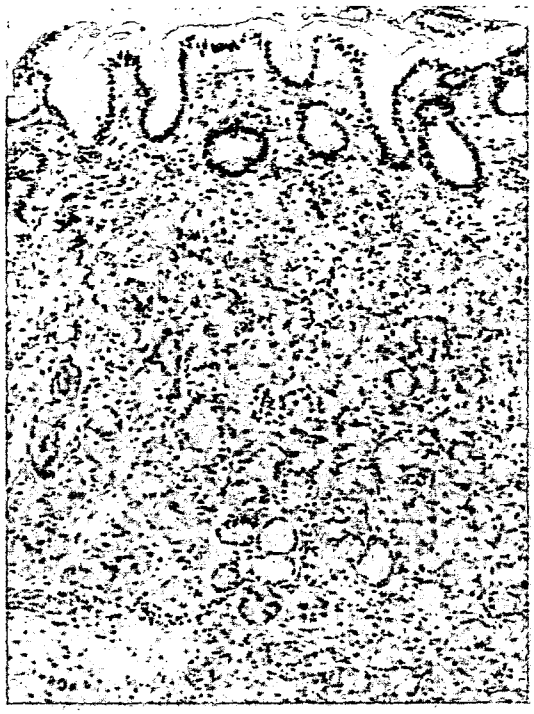

Fig. 6 Biopsy specimen from a nodule in the gastric body did not show a subepithelial collagen band or marked infiltration of inflammatory cells in the lamina propria. (H&E; original magnification, ×20.)

Fig. 7 Biopsy specimen from mucosa near the nodule showed a thickened 50- to 100-μm collagen band and prominent infiltration of the inflammatory cells. The focal epithelial surface was damaged and partially detached. Mild atrophy was observed, with a form of pseudopyloric gland. (H&E; original magnification, ×20.)

spread widely to all of the greater curvature of the gastric body and antrum. The nodular appearance is caused not by swollen mucosa, but depressed mucosa surrounding the nodules. By focusing on the specific nodular pattern we could identify more cases of collagenous gastritis.

Histologically, collagenous gastritis and the more frequently reported collagenous colitis are both characterized by the combination of a subepithelial collagenous band with an inflammatory infiltrate in the mucosa. Although the subepithelial deposit in collagenous colitis tends to spread diffusely and continuously, collagenous deposition and inflammatory infiltrate tend to vary and are often irregular in collagenous gastritis. The glandular structure was well preserved in the nodule, while in the surrounding mucosa, inflammatory infiltrates were remarkable and destructive to glands. These findings suggest that nodularity results from the irregular destruction of mucosal glands due to patchy inflammation; however, it remains unknown why the degree of mucosal inflammation is heterogeneous. In contrast, collagenous colitis shows few findings on endoscopy and no sign of mucosal nodularity, possibly resulting from homogeneous inflammation and diffuse collagen deposition.

The course and prognosis of collagenous gastritis also remain unknown. There are three reports describing endoscopic and histologic follow-up studies of collagenous gastritis: Pulimood *et al.* [7] reported a patient with increased thickness of a collagen band over 4 years, but the cellularity of the lamina propria and the degree of atrophy were similar to those seen in the initial samples. Upper endoscopy 6 years after the initial examination continued to show diffuse nodularity. Lagorce-Pages *et al.* [12] reported a moderate decrease in the thickness of the subepithelial collagen band in a biopsy sample obtained 8 years after the initial diagnosis, but the cellularity of the lamina propria was similar to that seen in the initial samples. Winslow *et al.* [17] reported the 12-year clinicopathological follow-up of a patient. The gastric body mucosa had a nodular appearance on the initial and subsequent endoscopic examinations, whereas the antral mucosa appeared normal. Gastric body biopsy specimens showed patchy, chronic active gastritis with gradual progression in disease severity over the 12-year period, although the collagen bands did not appear to become more diffusely distributed or thicker over time. In our case the nodular appearance became more conspicuous and extended to the antrum endoscopically, in addition to a more thickened collagen band histologically, over 14 years. As the histological findings differ between specimens taken from the nodules and those taken near the nodules, it is difficult to compare the collagen band thickness among biopsy specimens in detail; however, we speculate that the endoscopic and histological

Fig. 8 A biopsy specimen from the mucosal nodularity of the gastric body 14 years previously showed a thickened collagen band averaging 20 μm and inflammation. (H&E; original magnification, ×40.)

findings of this disease progress gradually over a long-term period.

Lagorce-Pages *et al.* divided patients with collagenous gastritis into two groups [12]: (1) children and young adults presenting with abdominal pain and disease limited to the gastric mucosa and (2) adult patients presenting with chronic watery diarrhea associated with collagenous colitis. Our case seems to belong to the group of children and young adults, because there were no findings of diarrhea or collagenous colitis. Young patients often show a gastric nodular pattern on endoscopy; in contrast, adult cases show mucosal erythema or no remarkable findings [12] except for the case of a 35-year-old woman presenting with a nodular pattern [6]. Although the histological findings are similar to those in the young adult group, it is unclear why the adult does not show mucosal nodularity. Freeman reported the case of a 74-year-old woman presenting with mucosal erythema and loss of vascular pattern in the gastric antrum [10]. Histological deposits of collagen were present diffusely throughout the biopsies. Lagorce-Pages *et al.* [12] described that the collagen band tended to vary and was often irregular in adult cases without nodularity. It is possible that loss of nodularity results from homogeneous inflammation and diffuse collagen deposition, and the distribution of inflammatory infiltrate and collagen deposits should therefore be evaluated by multiple biopsies in adult cases. The adult group is characterized by the simultaneous occurrence of collageneous colitis and duodenitis, but no nodular appearance is observed in the mucosa of the colon and duodenum [12]. It is therefore possible that collagenous gastritis in the adult group is part of a diffuse disorder involving the entire gastrointestinal tract [18], while in the young group the collagenous band is limited to the stomach, without duodenal or colonic involvement. The cause and pathogenesis of collagenous gastritis in the young group might therefore differ from that in the adult group. Whether pediatric and young adult patients transition to the adult group with age is very interesting. Pulimood *et al.* reported a young adult man with collagenous gastritis who developed collagenous colitis 6 years later [7]. Our case was followed up without medication, and he has no symptoms 3 years after diagnosis.

References

1. Colletti RB, Trainer TD (1989) Collagenous gastritis. Gastroenterology 97:1552–1555
2. Borchard F, Niederau C (1989) Kollagene gastrodudenitis. Dtsch Med Wochenschr 114:1345
3. Freeman HJ, Piercey JRA, Raine RJ (1989) Collagenous gastritis. Can J Gastroenterol 3:171–174
4. Cote JF, Hankard GF, Faure C, Mougenot JF, Holvoet L, Cezard JP, Navarro J, Peuchmaur M (1998) Collagenous gastritis revealed by severe anemia in a child. Hum Pathol 29:883–886
5. Stolte M, Ritter M, Borchard F, Koch-Scherrer G (1990) Collagenous gastroduodenitis on collagenous colitis. Endoscopy 22:186–187
6. Groisman GM, Meyers S, Harpaz N (1996) Collagenous gastritis associated with lymphocytic colitis. J Clin Gastroenterol 22:134–137
7. Pulimood AB, Ramakrishna BS, Mathan MM (1999) Collagenous gastritis and collagenous colitis: a report with sequential histological and ultrastructural findings. Gut 44:881–885
8. Castellano VM, Muñoz MT, Colina F, Nevado M, Casis B, Solis-Herruzo JA (1999) Collagenous gastrobulbitis and

collagenous colitis. Case report and review of the literature. Scand J Gastroenterol 34:632–638
9. Vesoulis Z, Lozanski G, Ravichandran P, Esber E (2000) Collagenous gastritis: a case report, morphologic evaluation, and review. Mod Pathol 13:591–596
10. Freeman HJ (2001) Topographic mapping of collagenous gastritis. Can J Gastroenterol 15:475–478
11. Stancu M, De Petris G, Palumbo TP, Lev R (2001) Collagenous gastritis associated with lymphocytic gastritis and celiac disease. Arch Pathol Lab Med 125:1579–1584
12. Lagorce-Pages C, Fabiani B, Bouvier R, Scoazec JY, Durand L, Flejou JF (2001) Collagenous gastritis: a report of six cases. Am J Surg Pathol 25:1174–1179
13. Kajino Y, Kushima R, Koyama S, Fujiyama Y, Okabe H (2003) Collagenous gastritis in a young Japanese woman. Pathol Int 53:174–178
14. Wang HL, Shah AG, Yerian LM, Cohen RD, Hart J (2004) Collagenous gastritis, an unusual association with profound weight loss. Arch Pathol Lab Med 128:229–232
15. Park S, Kim DH, Choe YH, Suh YL (2005) Collagenous gastritis in a Korean child: a case report. J Korean Med Sci 20:146–149
16. Dixon MF, Genta RM, Yardley JH, Correa P (1996) Calssification and grading gastritis, the updated Sydney system. Am J Surg Pathol 20:1161–1181
17. Winslow JL, Trainer TD, Colletti RB (2001) A long-term follow-up with the development of endocrine cell hyperplasia, intestinal metaplasia, and epithelial changes indeterminate for dysplasia. Am J Clin Pathol 116:753–759
18. Freeman HJ (2005) Collagenous mucosal inflammatory diseases of the gastrointestinal tract. Gastroenterology 129:338–350

Oncogene (2007), 1–11

www.nature.com/onc

ORIGINAL ARTICLE

Lack of Bcl11b tumor suppressor results in vulnerability to DNA replication stress and damages

K Kamimura[1], Y Mishima[1,2], M Obata[1,2], T Endo[1], Y Aoyagi[1] and R Kominami[1,2]

[1]*Department of Molecular Genetics, Niigata University Graduate School of Medical and Dental Sciences, Niigata, Japan and* [2]*Center for Transdisciplinary Research, Niigata University, Niigata, Japan*

Bcl11b/Rit1 **is involved in T-cell development and undergoes chromosomal rearrangements in human T-cell leukemias. Thymocytes of** ***Bcl11b*** $^{-/-}$ **newborn mice exhibit apoptosis at a certain developmental stage when thymocytes re-enter into the cell-cycle. Here, we show that Bcl11b-knockdown T-cell lines, when exposed to growth stimuli, exhibited apoptosis at the S phase with concomitant decreases in a cell-cycle inhibitor, p27 and an antiapoptotic protein, Bcl-xL, owing to transcriptional repression. This repression was a likely consequence of the impairment of Sirt1, a nicotinamide adenine dinucleotide-dependent deacetylase associating with Bcl11b. Activation of the apoptotic process cleaved the mediator protein, Claspin, and inhibited phosphorylation of cell-cycle checkpoint kinase 1 (Chk1) that plays a central role in sensing and responding to incomplete replication.** ***Bcl11b*** $^{-/-}$ **thymocytes also failed to phosphorylate Chk1 when UV irradiated. These results implicate Bcl11b in the remedy for DNA replication stress and maintenance of genomic integrity.**

Oncogene advance online publication, 19 March 2007; doi:10.1038/sj.onc.1210388

Keywords: DNA replication stress; Chk1; p27; apoptosis; Bcl11b tumor suppressor

Introduction

Eucaryotic cells maintain genomic integrity by monitoring DNA for damage or incomplete replication. In the event of aberrant DNA structures being detected, cells activate regulatory pathways to delay cell-cycle progression and to allow the damage to be repaired or replication to be completed (Abraham, 2001). Cells can also activate pathways leading to apoptosis and the removal of a damage cell from a tissue. The balance between the two pathways determines the survival of individual cells and the maintenance of genomic stability. Mammalian cells have two protein kinases of the phosphoinositide 3-kinase-related kinase family, ataxia telangiectasia mutated (ATM) kinase and ATM-Rad3-related kinase (ATR), which play central roles in sensing and responding to chromosomal insults (Abraham, 2001). Downstream of ATM and ATR kinases are the cell-cycle checkpoint kinases (Chk)1 and Chk2, activation of which requires the mediator family of proteins such as Claspin and BRCA1.

DNA replication stress occurring in S phase triggers activation of ATR that phosphorylates Chk1 at Ser317 and Ser345 and upregulates its kinase activity (Abraham, 2001; Chen and Sanchez, 2004). Activated Chk1 inhibits the protein phosphatase Cdc25A and Cdc25C by phosphorylation, halting ongoing DNA replication and initiating DNA repair. Cdc25A and Cdc25C control inhibitory phosphorylation sites on cyclin-dependent kinases (cdks), critical regulators of cell-cycle transitions (Walworth *et al.*, 1993; Sanchez *et al.*, 1997). As Chk1 has a critical role in maintaining genomic stability, Chk1 inactivation in somatic cells results in accumulation of structural chromosomal aberrations, eventually leading to tumorigenesis (Kastan and Bartek, 2004; Lam *et al.*, 2004). Consistently, study of *Chk1* knockout mice shows that *Chk1* is a haploinsufficient tumor suppressor gene (Lam *et al.*, 2004).

$p27^{Kip1}$, a cdk inhibitor, is a rate-determining component of cell-cycle exit in a number of cell types and plays a key role in coordinating the activity of cyclin E-cdk2 with accumulation of cyclin D-cdk4 (Nakayama *et al.*, 2004). The amount of p27 increases in quiescent cells, whereas mitogens and extracellular matrix adhesion signals can promote p27 degradation, allowing quiescent cells to re-enter the cell-cycle. Consistent with a role for p27 in cell proliferation, *p27* knockout mice develop hyperplasia in multiple organs but are relatively free from malignancy with the exception of pituitary hyperplasia (Fero *et al.*, 1996; Kiyokawa *et al.*, 1996; Nakayama *et al.*, 1996). Thus, p27 might act as a weak tumor suppressor of a narrowly defined group of cells, largely the decision of cells to exit the cell-cycle (Fero *et al.*, 1998; Di Cristofano *et al.*, 2001).

Bcl11b/Rit1/Ctip2 is a tumor suppressor gene isolated by positional cloning using γ-ray-induced mouse thymic lymphomas (Shinbo *et al.*, 1999; Wakabayashi *et al.*, 2003a; Sakata *et al.*, 2004). Recurrent chromosomal rearrangements at *BCL11B* locus are also found in

Correspondence: Dr R Kominami, Department of Molecular Genetics, Niigata University Graduate School of Medical and Dental Sciences and Center for Transdisciplinary Research, Niigata University, Asahimachi 1-757, Niigata 951-8510, Japan.
E-mail: rykomina@med.niigata-u.ac.jp
Received 23 August 2006; revised 1 February 2007; accepted 6 February 2007

human T-cell leukemias (Nagel *et al.*, 2003; Przybylski *et al.*, 2005). *Bcl11b* encodes a member of the zinc-finger proteins (Avram *et al.*, 2000; Satterwhite *et al.*, 2001; Wakabayashi *et al.*, 2003a) and directly interacts with Sirt1, a member of a third class of Trichostatin-resistant deacetylase, and with the nucleosome remodeling and histone deacetylase complex, one of the major transcriptional corepressor complexes in mammalian cells (Senawong *et al.*, 2003; Cismasiu *et al.*, 2005). However, target genes or genes controlled by *Bcl11b* are not known. *Bcl11b*$^{-/-}$ mice die soon after birth, exhibiting the developmental arrest of thymocytes of the $\alpha\beta$ T-cell lineage (Wakabayashi *et al.*, 2003b). Interestingly, their thymocytes retain normal cellularity relative to wild-type littermates at the DN3 (CD4$^-$ CD8$^-$ CD25$^+$ CD44$^-$) developmental stage; however, apoptosis and low cellularity are observed at the DN4 (CD4$^-$ CD8$^-$ CD25$^-$ CD44$^-$) stage, accompanying with decrease of an antiapoptotic protein, Bcl-xL (Inoue *et al.*, 2006). At the DN4 stage, thymocytes re-enter into the cell-cycle and rapidly proliferate (Gounari *et al.*, 2001; van de Wetering *et al.*, 2002). As apoptosis has been considered as a mechanism to eliminate deleterious cells, the apoptotic phenotype of *Bcl11b*$^{-/-}$ thymocytes seems to contradict with Bcl11b as a tumor suppressor.

This article examines Bcl11b-lacking cells *in vitro* and *in vivo* to elucidate how the apoptosis conferred by Bcl11b deficiency contributes to tumor development. Here, we show growth stimulation-dependent apoptosis and Chk1 deregulation in those cells, suggesting a role of Bcl11b in the remedy for stress during DNA replication and maintenance of genomic stability.

Results

Growth suppression and apoptosis of Bcl11b-KD cells

Bcl11b knockdown (KD) lines were produced by transfecting plasmid DNA expressing two different short interfering RNA (siRNA) sequences into Jurkat cells, a human T-cell lymphoma line. Figure 1a shows Western blots of three KD cell lines derived from transfectants using one siRNA and Supplementary Figure S1 shows those of the other. Marked decrease in the Bcl11b expression was seen in KD lines (si-1, -2, -3), compared with two control cell lines (sc-1, -2) that were obtained with plasmid DNA expressing scramble RNA sequences. 3-(4,5-Dimethylthiazol-2-yl)-2,5-diphenyltetrazolium bromide (MTT) assay revealed repression of cell growth in all KD lines relative to control lines under the condition of 10% serum supplementation, whereas such difference was not observed at 5 or 1% serum concentration (Figure 1b). Analyses of apoptosis in 10% serum-supplemented KD cells displayed elevated proportions of Annexin V-positive cells (Figure 1c) and terminal deoxynucleotidyl transferase biotin-dUTP nick end labeling (TUNEL) staining-positive cells (Figure 1d). Consistently, cleavage of caspase-7 and decrease in expression of an antiapoptotic protein, Bcl-xL (Motoyama *et al.*, 1995), were detected (Figure 1a). This apoptotic phenotype is consistent with that in *Bcl11b*$^{-/-}$ mouse thymocytes (Wakabayashi *et al.*, 2003b; Inoue *et al.*, 2006) and may contrast with the current notion that apoptosis is reduced when tumor suppressor gene is lost.

We examined cell cycling after the release from double-thymidine block. At 10% serum concentration, most cells entered into S phase 6 h after the release but KD cells showed some delay in cell-cycle progression. It was noted that the number of the S phase cells was much lower in KD cells than control cells, whereas the number of sub-G1 phase cells was higher (Figure 1e). This suggests the abrogation of S phase checkpoint in KD cells and resulting apoptosis of some KD cells. On the other hand, analysis at 5% serum concentration revealed slowing down of cell-cycle progression in both KD and control cell lines. Of note is that no sub-G1 cells were detected in KD cells, indicating absence of apoptosis (Figure 1e). These results indicate that at 10% serum concentration, Bcl11b down regulation causes inhibition of cell growth owing to apoptosis and implicate the *Bcl11b* gene in S phase checkpoint.

S phase damage response

DNA replication and UV-induced DNA damages generate single-stranded DNA (ssDNA), which serves as the signal for S phase checkpoint (Zou and Elledge, 2003). We thus examined the effect on cell growth and cell cycling of KD cells after treatment with UV. We also examined effects of Camptothecin, an inhibitor of topoisomerase I and γ-ray. Camptothecin produces both ssDNA and double-stranded DNA breaks (DSBs), whereas γ-ray generates DSBs (Kastan and Bartek, 2004; Flatten *et al.*, 2005). At 10% serum concentration, UV and Camptothecin-inhibited cell growth more markedly for KD cells, whereas ionizing radiation inhibited both KD cells and control cells equally

Figure 1 Downregulation of *Bcl11b* inducing cell growth retardation and apoptosis. (a) Western blot shows cleavage of procaspase-7 and decrease in the protein level of BclxL in 10% serum-supplemented Jurkat cells when Bcl11b is downregulated by siRNA. (b) Cell numbers shown at indicated times: KD cells treated with siRNA (closed circles: si-1, squares: si-2 and triangles: si-3) and control cells with expression of Bcl11b (open circles: Jurkat cells, squares: sc-1 and triangles: sc-2). Bcl11b-downregulated cells show slower cell growth than control cells in the 10% serum medium but the difference disappears in the 5 or 1% serum medium. (c) Flow cytometric analysis of cells stained with Annexin V from indicated cell lines. The profile of normal Jurkat cells is displayed in black line. (d) TUNEL staining of Jurkat cells. The sc-1 and si-2 cells were treated with the TdT enzyme and stained with dUTP-fluorescein isothiocyanate using a TUNEL staining kit (Takara Inc., Japan), counterstained with 4′,6-diamidino-2-phenylindole, dihydrochloride. (e) Cell-cycle analysis of cells at indicated times after the release from double thymidine block. The numbers of S phase cells 6 h after the release decreases in 10% serum-supplemented KD cells whereas the numbers of sub-G1 phase cells increases. In 5% serum-supplemented cells, the number of S phase cells 8 h after the release decreases but the number of sub-G1 phase cells does not increase.

(Figure 2a). The sub-G1 fraction was increased in KD cells over control cells after UV and Camptothecin treatments whereas the levels of the increase were similar for control and KD cells when exposed to γ-rays (Figure 2b).

Cell-cycle analysis of control cells showed persistence in the number of S phase cells 3 h after UV irradiation, indicating arrest in the cell-cycle progression (Figure 2c). In contrast, a decrease of S phase cells was observed in KD cells. These indicated impaired activation of S phase

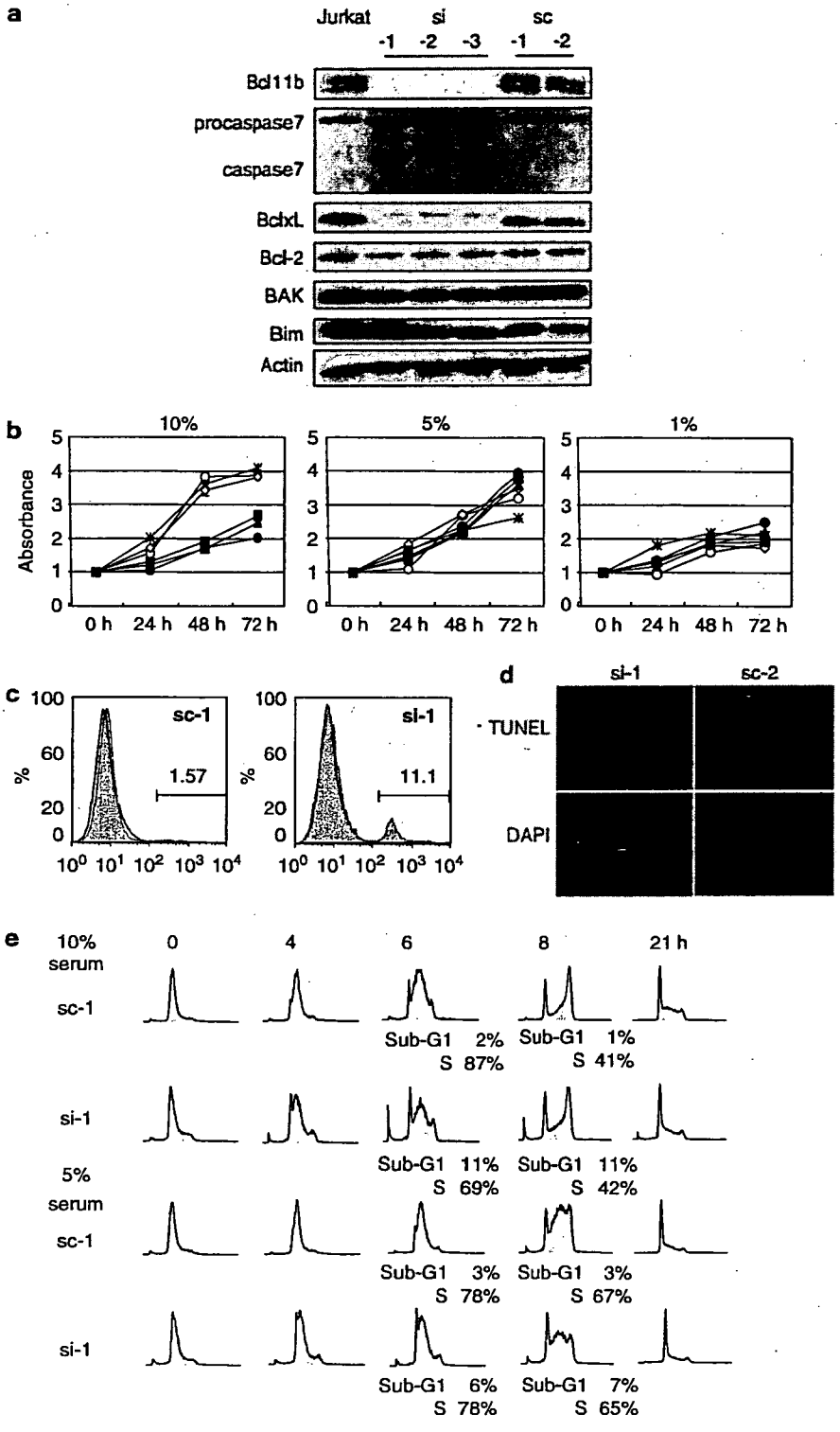

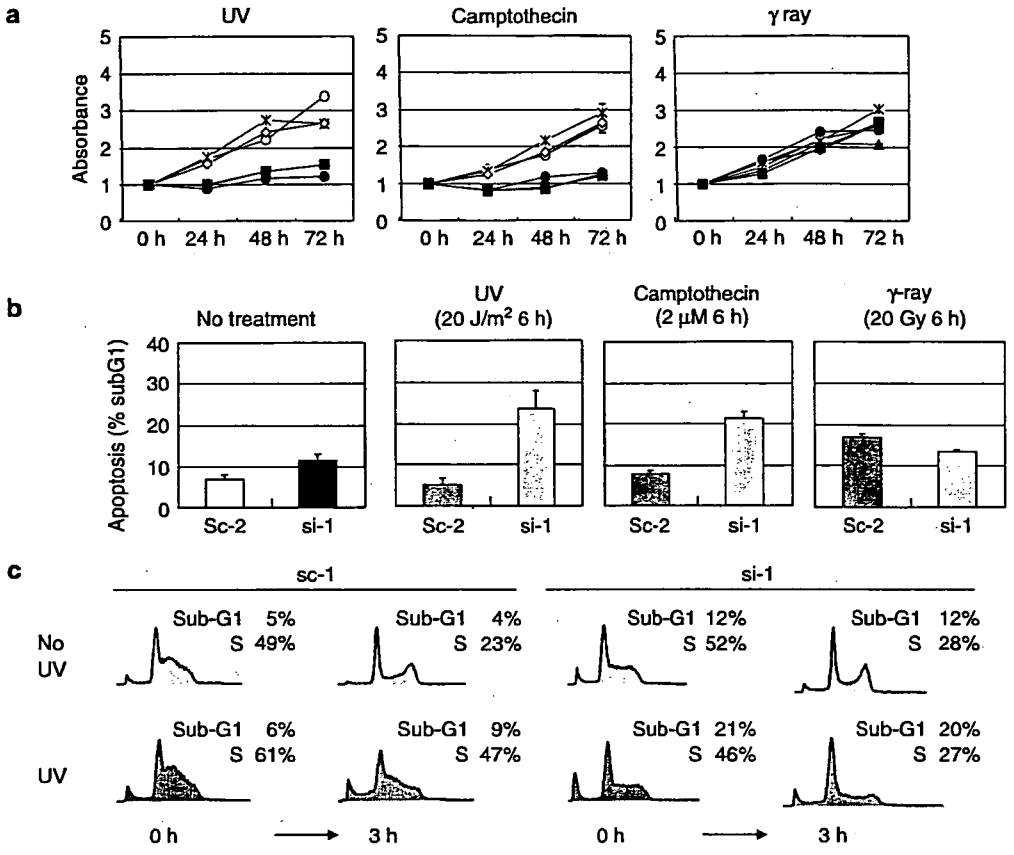

Figure 2 Impairment of S phase checkpoint. (**a**) Cell numbers shown at indicated times. The pattern of control cells is displayed in Figure 1b. Bcl11b-KD cells (closed circles, squares and triangles) are more susceptible to UV and Camptothecin than control cells (open circles, squares and triangles). That difference in susceptibility is not seen for γ-irradiation. (**b**) Summary of percents of sub-G1 phase cells in sc-2 and si-1 cells after exposure to UV, Camptothecin and γ-ray. (**c**) Cell-cycle analysis shows the abrogation of S phase checkpoint in KD cells. Six hours after the release from double thymidine block, cells were treated with UV (UV-C, 20 J/m²) and analysed with flow cytometer 3 h after. Arrest at S phase is seen in sc-1 control cells but not in si-1 cells.

checkpoint and enhanced apoptotic response in 10% serum-supplemented KD cells.

Impairment of Chk1 phosphorylation

The ssDNA damages activate ATR and its downstream checkpoint kinases, Chk1 and Chk2 (Liu *et al.*, 2000; Abraham, 2001). We thus examined these checkpoint kinases in 10% serum-supplemented KD cells before and after UV irradiation. Figure 3a shows examples of Western blotting and Figure 3b summarizes the results. Expression of Chk1 protein did not differ between control and KD cells, and UV irradiation did not affect their protein expression. However, the phosphorylation level of Chk1 was very low in KD cells, and UV irradiation did not elevate the phosphorylation level as did in control cells. Cdc25A, a substrate of Chk1 (Zhao *et al.*, 2002), showed a high expression in KD cells, indicating the inhibition of degradation owing to Chk1 impairment. On the other hand, expression and phosphorylation levels of Chk2 did not differ between KD and control cells and were not affected by UV irradiation. These results indicated Bcl11b downregulation resulting in the impairment of Chk1 phosphorylation but such effect on Chk2 phosphorylation was unclear because the phosphorylation levels were not affected even in parental Jurkat or control sc-1 cells. Subcellular localization of Bcl11b and Chk1 was examined by fractionating protein extracts from Jurkat cells (Figure 3c). Most Bcl11b proteins were present in the chromatin-bound (Ch) fraction and this was not affected by UV irradiation. On the other hand, Chk1 and phosphorylated Chk1 at S317 existed in the cytoplasmic and Ch fractions. Interestingly, after UV irradiation, phosphorylated Chk1 at S317 was localized in the soluble nuclear fraction whereas phosphorylated Chk1 at S345 in the soluble nuclear and also cytoplasmic fractions. The molecular basis for this difference is not clear. These results suggest different responsiveness of Bcl11b and phosphorylated Chk1 to UV irradiation.

Chk1 phosphorylation was also examined in 5% serum-supplemented KD cells, as no difference in cell growth was observed between control and KD cells (Figure 1b). Western blot revealed no difference in the phosphorylation level between KD and control cells (Figure 3d), indicating restoration of S phase checkpoint

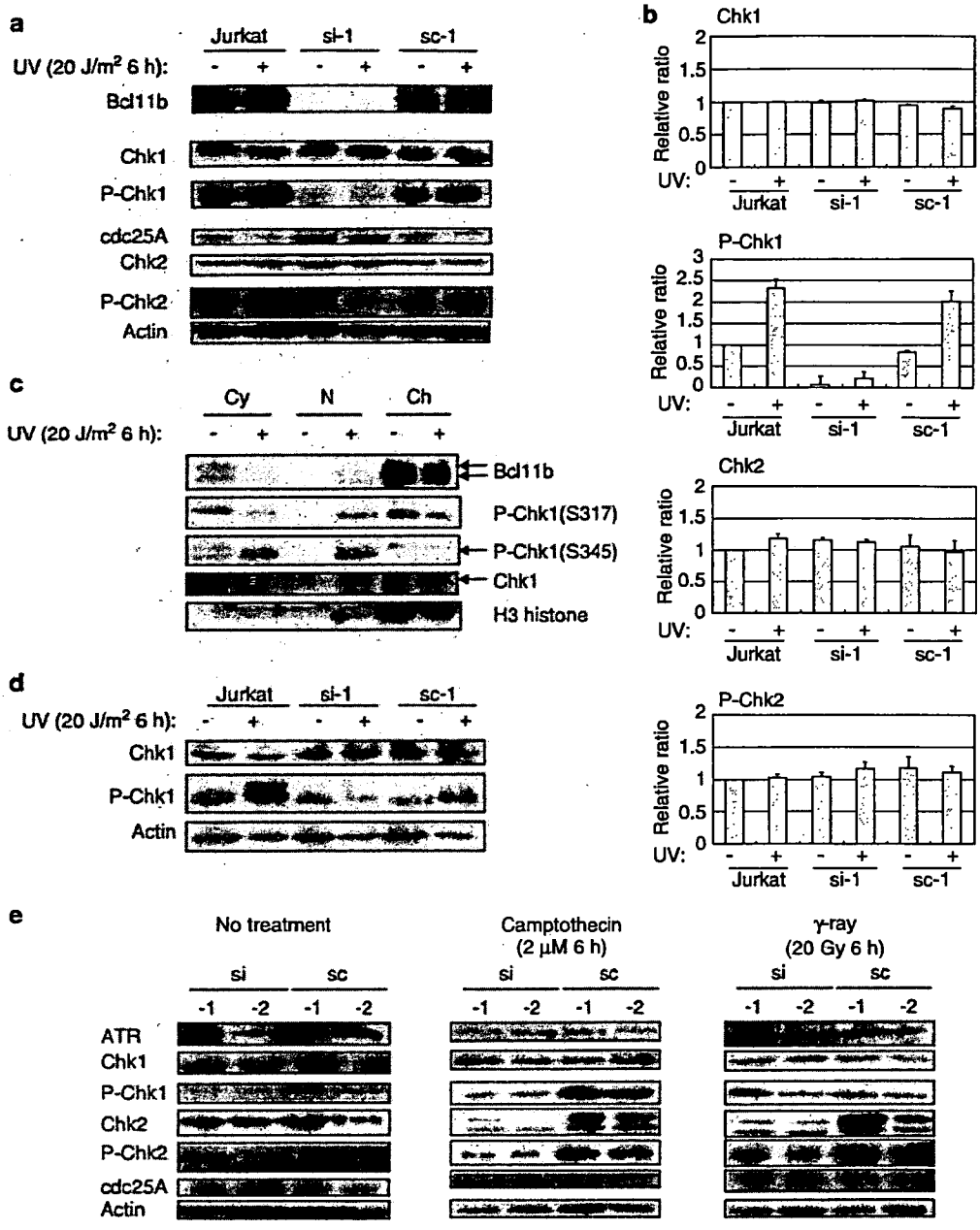

Figure 3 Effects of UV, Camptothecin and γ-ray on Chk1 and Chk2. (**a**) Western blotting of Chk1 and Chk2 proteins in 10% serum-supplemented cells. Decreased phosphorylation of Chk1 at Ser317 is seen in si-1 cells and the phosphorylation level does not increase in response to UV irradiation. Consistently, the expression of cdc25 is high in si-1 cells. No difference between control and KD cells is observed for Chk2. (**b**) Relative band ratios of Chk1, P-Chk1, Chk2 and P-Chk2 are shown, using the band intensities of β-actin as references. Results are expressed as mean and error bars show standard deviations of three independent experiments. (**c**) Subcellular localization of Bcl11b and Chk1 in Jurkat cells. Protein extracts in cytoplasmic, soluble nuclear and Ch fractions were probed with antibodies against Bcl11b, Chk1, phosphorylated Chk1 at S317 and S345 and histone H3. Bcl11b and phosphorylated Chk1 are mainly localized at the chromatin but they are differently fractionated in UV-irradiated cells. (**d**) Western blots in 5% serum-supplemented cells. The phosphorylation level of Chk1 in si-1 cells is similar to that in sc-1 cells but does not increase in response to UV irradiation. (**e**) Chk1 and Chk2 phosphorylation after exposure to Camptothecin and γ-ray. The phosphorylation level of Chk1 at Ser317 increases 6 h after administration of Camptothecin in control cells (sc-1 and sc-2) but not in KD cells (si-1 and si-2). Also, the phosphorylation level of Chk2 does not increase in si-1 and si-2 cells in response to UV irradiation. On the other hand, exposure of si-1 and si-2 cells to γ-ray affects the phosphorylation of Chk2 but not Chk1. Collectively, impairment in Chk1 phosphorylation only is seen for UV irradiation, impairment in the phosphorylation of both Chk1 and Chk2 is seen for Camptothecin treatment and impairment in Chk2 phosphorylation only is seen for γ-ray irradiation.

under this culture condition. However, UV irradiation did not increase the Chk1 phosphorylation in KD cells. This suggests that the Bcl11b-lacking state provides a latent defect in S phase checkpoint which is revealed by growth stimuli and/or UV irradiation.

Figure 3e shows effect of Camptothecin and γ-irradiation. Administration of Camptothecin in KD cells exhibited impairment of phosphorylation for both Chk1 and Chk2 probably owing to generation of ssDNA and DSBs whereas the impairment was seen only for Chk2 after γ-ray producing DSBs. The results revealed inability of Bcl11b-KD cells to activate both Chk1 and Chk2 in response to DNA-damaging agents. Among other proteins involved in ATR/Chk1 signaling pathway, expression of Claspin was found to decrease in 10% serum-supplemented KD cells (Supplementary Figure S2). As Claspin is required for activation of Chk1 by ATR (Lin *et al.*, 2004), this decrease may be relevant for reduced phosphorylation of Chk1 in KD cells.

Apoptosis, deregulated cell-cycle checkpoint and Sirt1 connection

Recently, Clarke *et al.* (2005) reported that Claspin is a specific substrate of caspase-7 and cleaved during the initiation of genotoxic stress-induced apoptosis and that the Claspin processing regulates Chk1 activity. Accordingly, the Claspin cleavage may account for our finding of impaired Chk1 phosphorylation in 10% serum-supplemented KD cells. We thus performed Western blotting of caspase-7, Claspin, Chk1 in KD cells harvested at various times after shifting from 5 to 10% serum. Also, Bcl-xL and p27 were examined, because the serum elevation triggers cell-cycle progression regulated by p27 (Nakayama *et al.*, 2004). The cleavage of caspase-7 was noted 3 h after the shift, followed by the degradation of Claspin and decrease of phosphorylated Chk1 (Figure 4a). This suggests a cascade of the activation of caspase-7, cleavage of Claspin and the inactivation of Chk1 kinase, consistent with that by Clarke *et al.* (2005). On the other hand, the amount of Bcl-xL was low to start with but markedly decreased 6 h after. p27 expression was also low in KD cells, though unexpectedly high in control Jurkat cells, and markedly decreased 3 h after. The p27 reduction probably results in a rapid G1 progression that may contribute to apoptosis under the low concentration of Bcl-xL.

Elevation of the serum concentration triggers PI3K/Akt kinase signaling and affects Sirt1 activity that associates with Bcl11b (Levine *et al.*, 2006). Thus, we examined Akt and Sirt1 by Western blotting (Figure 4b). No noticeable difference was seen in the level of Akt or phosphorylated Akt between the 10 and 5% serum concentrations. On the other hand, Sirt1 protein showed a substantial, though not marked, decrease in 10% serum-supplemented KD cells. The amount of another Bcl11b-associated protein, metastasis-associated protein 1 (Mta1) (Bagheri-Yarmand *et al.*, 2004; Cismasiu *et al.*, 2005), also decreased.

Sirt1 affects expression of a Foxo3a-target gene, *p27*, at the transcription level (Brunet *et al.*, 2004; Motta *et al.*, 2004). As Sirt1 proteins decreased in 10% serum-supplemented KD cells, we examined mRNA expression of *p27* and other genes presumably regulated by Foxo3a and Sirt1 in KD cells at various times after the serum shift. Semiquantitative reverse transcription–polymerase chain reaction (RT–PCR) showed that the mRNA level of *p27* decreased in KD cells 3 h after whereas the expression of *Bcl-xL* was low to start with and gradually decreased up to 24 h (Figure 4c). However, the levels of other possible Foxo3a-targets, *Bim* and *Gadd45*, were not affected. These suggest that growth stimulation by the serum elevation provides transcriptional repression of *p27* and *Bcl-xL* in *Bcl11b* KD cells but not in control *Bcl11b*-proficient cells.

Examination of cell line specificity

To test whether the Chk1 activation by Bcl11b is cell-line specific, we produced the FRSK skin keratinocyte cell line (tet-1) that expressed Bcl11b siRNA driven by a tetracycline/doxycycline inducible promoter. Western blotting showed a decrease in the expression of Bcl11b in tet-1 cells after addition of doxycycline but not in a control cell line (c-1) that was obtained by using plasmid DNA expressing scramble RNA sequences (Figure 5a). MTT assay exhibited repression of cell growth in the tet-1 cells in the presence of doxycycline (open circles) (Figure 5b). UV irradiation enhanced the growth repression, as in Bcl11b-KD Jurkat cells. Western blots showed a minimal decrease in Chk1 phosphorylation in the tet-1 cells with doxycycline but the decrease was prominent after UV irradiation (Figure 5a). The Bcl11b downregulation and UV irradiation also seemed to affect Chk2 and its phosphorylation but those effects were not marked. These results showed that the suppression of Chk1 phosphorylation by Bcl11b downregulation was also detected in FRSK cells.

Next, we examined mouse thymocytes *in vivo*. Thymocytes isolated from *Bcl11b*$^{+/+}$, *Bcl11b*$^{+/-}$ and *Bcl11b*$^{-/-}$ mice were incubated in the culture medium, irradiated with UV and examined for protein expression 18 h after. Figure 6a shows examples of Western blotting and Figure 6b summarizes the results. Reduced expression of p27 was observed in Bcl11b$^{-/-}$ thymocytes and the expression was restored to the control level by UV irradiation. The cleavage of Claspin was seen in Bcl11b$^{-/-}$ thymocytes and was enhanced by UV irradiation. On the other hand, protein levels of Chk1 or Chk2 did not differ in thymocytes between the three different *Bcl11b* genotypes, nor were they affected by UV irradiation. However, Bcl11b deficiency reduced phosphorylation of Chk1 at the S317 and S345 positions and also phosphorylation of Chk2. In addition, UV-induced phosphorylation of Chk1 much less in *Bcl11b*$^{-/-}$ thymocytes than in control thymocytes. Fivefold amount of protein extracts from irradiated *Bcl11b*$^{-/-}$ thymocytes allowed us to detect phospholylated Chk1. On the other hand, UV irradiation-induced phosphorylation of Chk2 in thymocytes of all the three different genotypes. p53

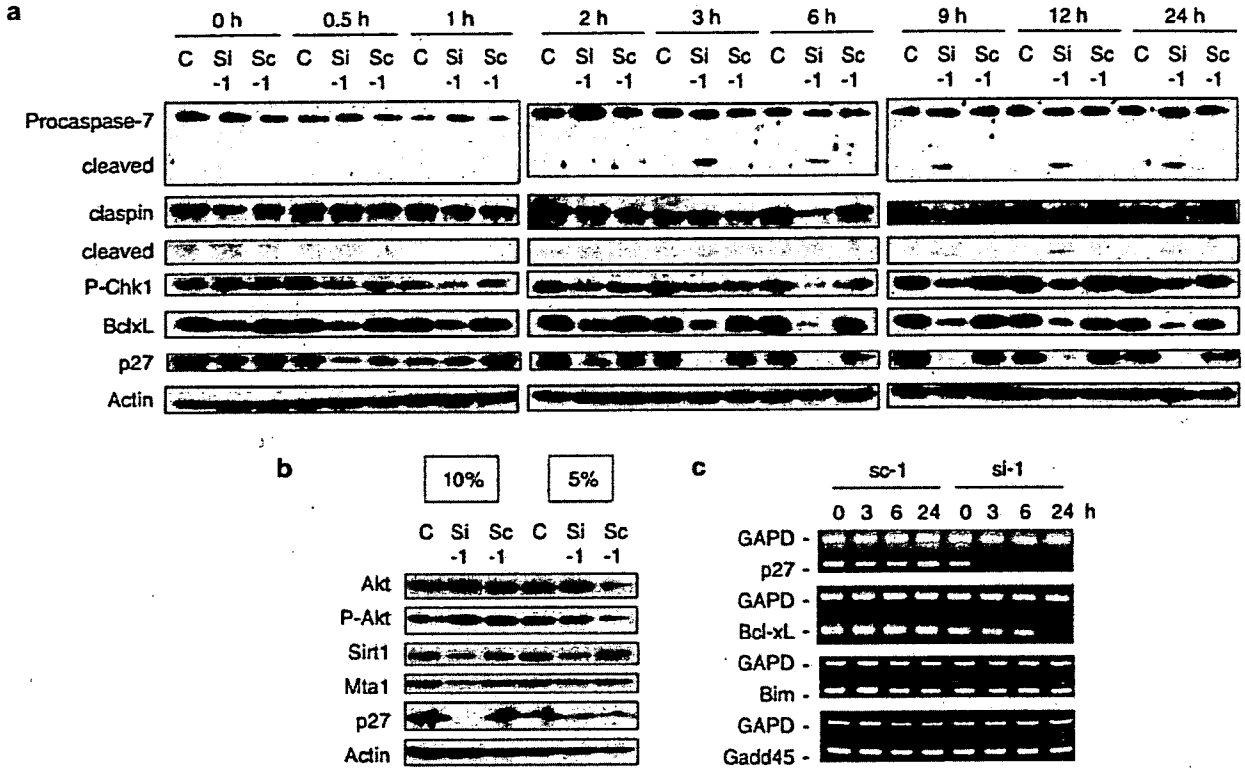

Figure 4 Changes of various proteins and RNA in Bcl11b-KD cells after growth stimulation. (**a**) Western blots of cells harvested at indicated times after changing the medium containing 5%–10% serum. Cleavage of procaspase-7 is noted 3 h after the change, and decreases in Claspin and phosphorylated Chk1 at Ser317 are seen 6 h after. Bcl-xL is low at the beginning and markedly decreases 3–6 h after and p27 decrease starts at 2 h after. (**b**) Western blots of Akt, Sirt1, Mta1 and p27 in 10 and 5% serum-supplemented cells. Expression or phosphorylation level of Akt on the mammalian target of rapamycin signaling pathway does not change. Expression levels of Sirt1, Mta1 and p27 proteins are lower in si-1 cells than sc-1 cells in the medium containing 10% serum. The difference is much less in that containing 5% serum. (**c**) RT–PCR analysis of cells harvested at indicated times after the medium change. The mRNA amount of *p27* rapidly decreases 3 h after whereas that of *Bcl-xL* is low at the beginning and gradually decreases until 24 h after. No change is seen in *Bim* or *Gadd45* mRNAs.

proteins in Bcl11b$^{-/-}$ thymocytes increased in response to UV irradiation. These results indicate that Bcl11b downregulation or deficiency leads to decrease of p27 and suppression of Chk1 phosphorylation both *in vitro* and *in vivo*.

Discussion

This paper shows that Bcl11b-KD T-cell lines, when exposed to growth stimuli or UV radiation, exhibited extensive apoptosis with concomitant decreases in p27 and Bcl-xL. Also, deregulation of Chk1 phosphorylation was observed in the KD cells and *Bcl11b*$^{-/-}$ thymocytes after UV irradiation. These implicate Bcl11b in resisting DNA replication stress or DNA damages, although it is not clear how Bcl11b remedies these stresses. Bcl11b directly interacts with Sirt1 deacetylase (Senawong *et al.*, 2003), and hence the Bcl11b deficiency may affect some Sirt1 activity. In fact, the amount of Sirt1 decreased in Bcl11b-KD cells relative to parental Jurkat cells where most Bcl11b proteins were localized at the chromatin. Sirt1 downregulates Foxo transcription factors but does not regulate all Foxo target genes in the same manner in different cellular contexts, because target genes such as *p27* and *Gadd45* are upregulated by Sirt1 in Foxo3a-expressing fibroblasts whereas another target of *Bim* gene is not affected (Brunet *et al.*, 2004; Motta *et al.*, 2004). Similar differential regulation was observed for Bcl11b in Jurkat cells. In 10% serum-supplemented Bcl11b-KD cells, *p27* expression decreased whereas expression of *Bim* or *Gadd45* was not affected. In addition, decreased expression of *Bcl-xL* was observed in those cells. Therefore, Bcl11b may affect a subset of Foxo target genes through Sirt1 activity, and these affected genes overlap with but are different from those of Sirt1 in the absence of Bcl11b. Activity of the Foxo factors is not only regulated through acetylation but also through phosphorylation by Akt (Levine *et al.*, 2006). However, this possibility is less likely in KD cells because the phosphorylation level of Akt did not increase in response to growth factor activation. Collectively, decreases in p27 and Bcl-xL might account for all the enhanced apoptosis associated with Bcl11b deficiency.

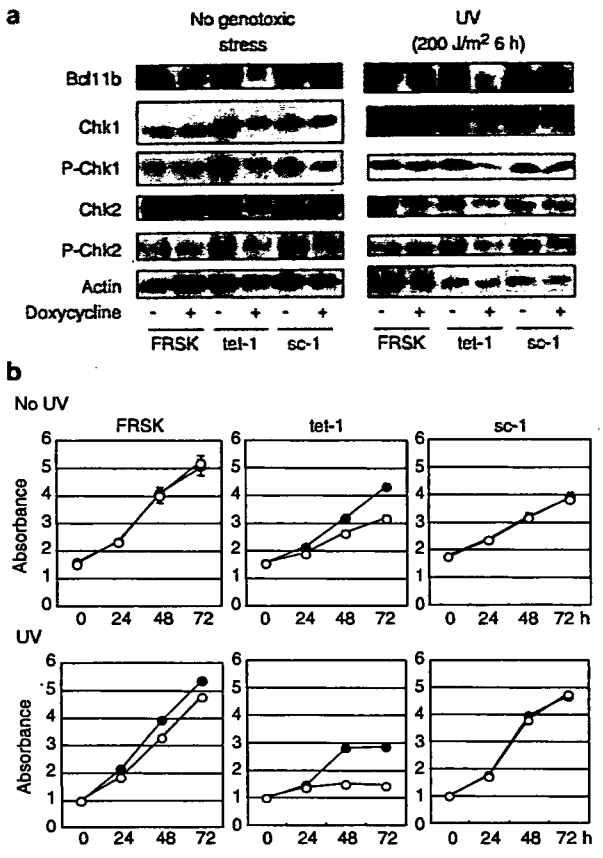

Figure 5 Bcl11b downregulation inhibits Chk1 phosphorylation in a keratinocyte cell line. (a) Western blot shows a decrease in the Bcl11b expression in tet-1 cells when doxycycline is added. The tet-1 cells under the presence of doxycycline phosphorylated Chk1 after UV irradiation much less than control cells. (b) The cell number is shown. In the presence of doxycycline (open circles), tet-1 cells, but not control c-1 cells, show slower cell growth than cells in the absence of doxycycline (closed circles). The difference in cell growth was prominent when UV and Camptothecin were treated.

Apoptosis has been considered as a mechanism to eliminate deleterious cells with DNA damages and hence apoptotic phenotype of the KD cells and *Bcl11b*$^{-/-}$ thymocytes seems to contradict with Bcl11b as a tumor suppressor. However, hyperplastic or dysplastic cells often exhibit apoptotic phenotype together with high mitotic index (Bartkova *et al.*, 2005; Gorgoulis *et al.*, 2005). Therefore, the apoptotic phenotype may be a reflection of accumulation of DNA damages or a deregulated elevation in cell-cycle progression in those cells. Such precancerous cells probably develop a rapidly progressive tumor phenotype when they acquire the ability to escape apoptosis. Our preliminary analysis showed that apoptosiS prone Bcl11b-deficient cells are capable to develop tumors, as transfer of *Bcl11b*$^{-/-}$ fetal liver cells into severe combined immunodeficiency mice led to the development of lymphomas at a frequency of four out of 12 cases (data not shown). On the other hand, the present study suggests a concealed function of apoptosis, which positively contributes to tumorigenesis. The activation of caspase-7 resulted in the Claspin cleavage which downregulated phosphorylation of Chk1, consistent with the previous report (Clarke *et al.*, 2005). This deregulation of Chk1 leading to a high level of Cdc25A is likely to enhance replication-mediated DNA damage accumulation during inappropriate cell cycling, contributing to tumor progression (Walworth *et al.*, 1993; Sanchez *et al.*, 1997; Takai *et al.*, 2000; Lam *et al.*, 2004). A second possible consequence of apoptosis is a generation of chromosomal translocations through DSBs caused by apoptotic endonucleases, as exemplified in *Tel-AML1* translocations (Eguchi-Ishimae *et al.* 2001). These possibilities may be supported by that selective components of the apoptotic process can be activated, followed by recovery of a normal cellular phenotype in the absence of apoptotic morphology (Alam *et al.*, 1999; Hoeppner *et al.*, 2001; Reddien *et al.*, 2001).

Finally, it is known that Chk1 downregulation potentiates antimetabolites and topoisomerase inhibitors by depriving the cancer cells of the Chk1 defensive mechanism (Zhou and Bartek, 2004). Likewise, Bcl11b downregulation sensitizes Jurkat cells to Camptothecin. This suggests that not only Chk1 but also Bcl11b is a potential application target of inhibitors in cancer therapy.

Materials and methods

Mice and genotyping

Bcl11b$^{+/-}$ mice of BALB/c background used in this study were maintained under specific pathogen-free conditions in the animal colony of the Niigata University. *Bcl11b*$^{-/-}$ mice were obtained by mating *Bcl11b*$^{+/-}$ mice. Isolation of genomic DNA from brain and thymic lymphomas was carried out by standard protocols. Genotyping of *Bcl11b* was carried out as described previously (Wakabayashi *et al.*, 2003a; Sakata *et al.*, 2004). All animal experiments comply to the guidelines by the animal ethics committee for animal experimentation of Niigata University.

Cells

Jurkat cells (p53 deficient) were cultured in Roswell Park Memorial Institute 1640 medium (Sigma, St Louis, MO, USA) containing 10% fetal bovine serum and 100 U/ml penicillin and streptomycin. Two different fragments of 64 nucleotides for siRNA covering the nucleotide positions 646–667 and 1303–1324 (see the Supplementary Figure S2 legend) of human Bcl11b coding region and scramble 21nt-sequence were cloned into pSilencer 2.1-U6 neo (Ambion, Austin, TX, USA). These vectors were transfected into Jurkat cells using DMRIE-C followed by G418 selection. Three and two independent clones (si-1, -2 -3 and si-a, -b) were isolated from the 646–667 region and the 1303–1324 region, respectively, and used. As for the FRSK cells (p53 deficient), the tet-on operator was incorporated into the pSilencer 2.1-U6 neo clone, and this was co-transfected with a hygromycin marker. One of the three independent hygromycin-resistant clones was selected, which showed low spontaneous expression but high inducibility of siRNA expression upon treatment with doxycycline at the dose of 5 μg/ml. The tet-inducible FRSK cells were cultured in the medium containing 10% tet-approved fetal bovine serum

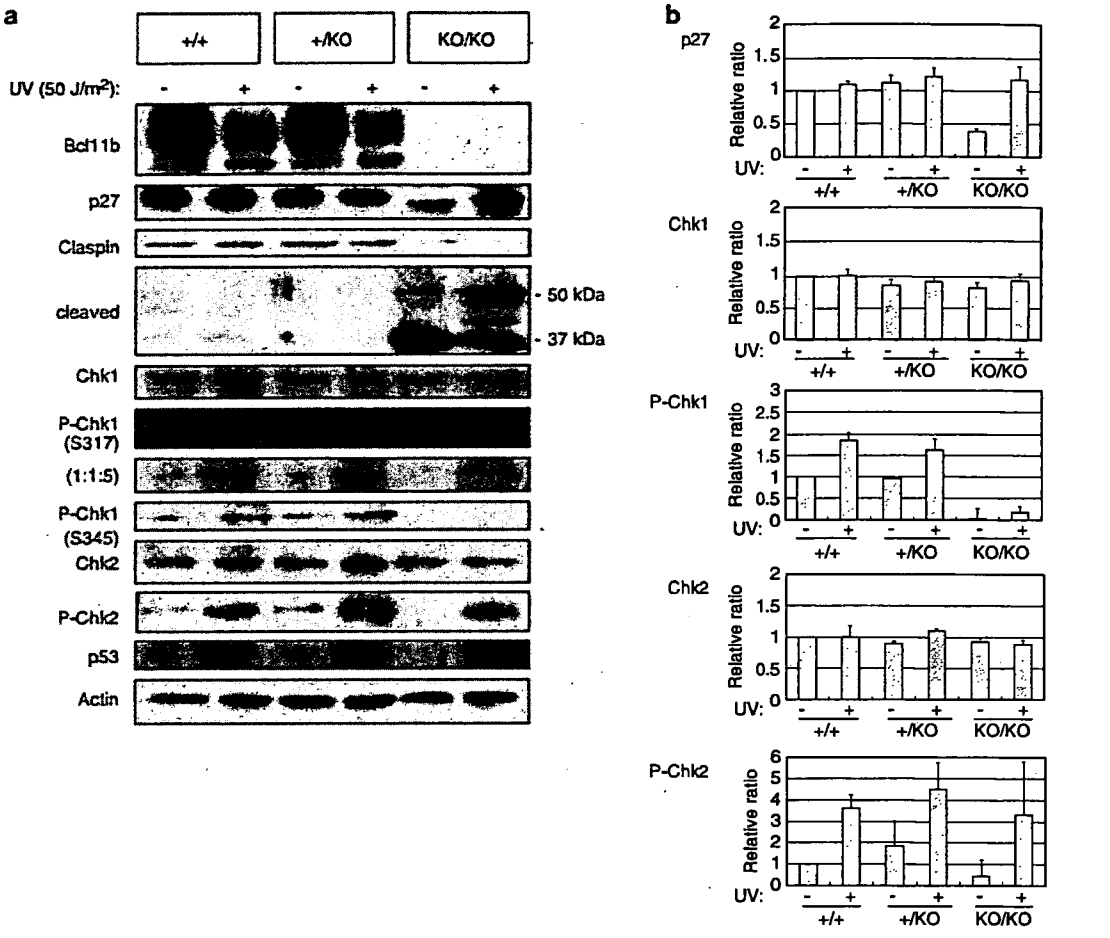

Figure 6 Deregulation of Chk1, but not Chk2, in *Bcl11b*$^{-/-}$ thymocytes. (**a**) Western blots show p27 reduction, degradation of Claspin and impairment of Chk1 phosphorylation at Ser317 and at Ser345 in *Bcl11b*$^{-/-}$ thymocytes. Increase in phosphorylation of Chk1 in response to UV irradiation is much less in *Bcl11b*$^{-/-}$ thymocytes than in *Bcl11b*$^{+/+}$ and *Bcl11b*$^{+/-}$ thymocytes. Fivefold amount of *Bcl11b*$^{-/-}$ thymocyte extracts provides a visible band of phospholylated Chk1. On the other hand, UV inducibility of phosphorylated Chk2 and p53 proteins is detected in *Bcl11b*$^{-/-}$ thymocytes. (**b**) Relative band ratios of p27, Chk1, P-Chk1, Chk2 and P-Chk2 are shown, using the band intensities of β-actin as references. Results are expressed as mean and error bars show standard deviations of three independent experiments.

(Clontech, Mountain View, CA, USA), 100 μg/ml of G418 and 50 μg/ml of hygromycin.

MTT cell growth assay

Jurkat cells were plated in 96-well tissue culture dishes at 5×10^4 cells per well in 100 μl of the medium and treated with and without UV, Camptothecin, or γ-ray. FRSK cells were treated in a similar manner in the medium containing doxycycline and in the medium without doxycycline. MTT reagents were added to the cells at the indicated times after the treatment, followed by counting with Premix WST-1 Cell Proliferation Assay System (Takara Inc., Kyoto, Japan).

Synchronization of cells and cell-cycle

Jurkat cells were incubated in the medium containing 0.56 mM thymidine (Sigma) for 18 h. After cultured for 15 h in thymidine-free medium, the cells were again incubated in the same medium for 15 h. Those cells were used for assays after the medium was removed. Six hours after the removal, cells were treated with UV and further incubated for indicated times. After washed in phosphate-buffered saline (PBS) and fixed in 70% ethanol, the cells were stained with propidium iodide, and subjected to analyses by FACSscan flow cytometer (BD Bioscience, San Jose, CA, USA), as described previously (Wakabayashi *et al.*, 2003b).

Detections of apoptosis

Apoptosis was analysed using Annexin V (BD Biosciences Clontech, Mountain View, CA, USA) by FACSscan flow cytometer (Becton Dickinson) according to the manufacture's protocol.

Fractionation into subcellular components

Jurkat cells were suspended in a buffer containing 0.2% NP-40 and fractionated as described (Andegeko *et al.*, 2001). Cytoplasmic fraction (Cy) was separated from nuclei by low-speed centrifugation, and the isolated nuclei were resuspended in the buffer containing 0.5% NP-40 and subjected to high-speed centrifugation to obtain soluble nuclear (N) and chromatin-bound (Ch) fractions. The proteins in each fraction

were separated by sodium dodecyl sulfate–polyacrylamide gel electrophoresis (SDS–PAGE) and duplicate membranes were blotted with antibodies against Bcl11b, Chk1, phosphorylated Chk1 at S317 and at S345 and histone H3.

Western blotting

Thymocytes and culture cells were suspended in PBS and mixed with an equal volume of lysis buffer, 0.125 M Tris–HCl (pH 6.8), 10% sucrose, 10% SDS, 10% 2-ME and 0.004% bromophenol blue. The extract was electrophoresed in 8 and 14% SDS–PAGE gels and blotted onto Hybond membranes (Amersham Pharmacia Biotech, Piscataway, NJ, USA). Antibodies used are listed below. Protein bands were visualized using chemiluminescent detection (ECL plus, Amersham Pharmacia Biotech).

Antibodies

Rabbit anti-Bcl11b-Z antibodies used in these experiments have been described previously (Wakabayashi *et al*., 2003b). Anti-caspase-7 (no. 9492), anti-Bcl-xL (no. 2762), anti-p27 Kip1 (no. 2552), anti-Akt (no. 9272), anti-Akt(pSer473) (no. 9271), anti-Chk1 (no. 2345), anti-Chk1(pSer317) (#2344), anti-Chk1(pSer345) (no. 2341), anti-Chk2 (no. 2662), anti-Chk2 (pThr68) (#2661), anti-cdc25A (no. 3652), anti-cdc25C (no. 922), anti-cdc25C(p216) (no. 9528), anti-ATR(pSer428) (no. 2853) and anti-p53 (no. 9282) were purchased from Cell Signaling Technology (Beverly, MA, USA). Anti-ATR (no. sc-1887), antiactin (no. sc-1615), anti-claspin (no. sc-27297), anti-BRCA1 (no. sc-6954), anti-Rad50 (no. sc-20155), anti-Rad9 (no. sc-10465), anti-Rad1 (no. sc-14314), anti-Hus1 (no. sc-8323), anti-MRE11 (no. sc-5859), anti-GADD45(#sc-797), anti-MTA1 (#sc-26654), anti-SIRT1 (no. sc-15404) and horse raddish peroxidase (HRP)-anti-goat immunoglobulin G (IgG) (#sc-2020) were purchased from Santa Cruz Biotechnology (Santa Cruz, CA, USA). Anti-NBS1 (#A300-187A) was purchased from Bethyl Laboratories (Montgomery, TX, USA). HRP-anti-rabbit IgG (no. NA934V) was purchased from Amersham Pharmacia Biotech.

RT–PCR

Total RNA was prepared from Jurkat cells using the RNA Easy Mini kit (Quiagen, Valencia, CA, USA) according to the protocol recommended by the manufacturer. cDNA was synthesized from 1–5 μg of total RNA with an oligo(dT) primer using SuperScript II reverse transcriptase (Invitrogen, Carlsbad, CA, USA) and an aliquot (1–2 of cDNA products) was used for PCR using primers listed below. Multiplex PCR was carried out similarly where glyceraldehyde-3-phosphate dehydrogenase (GAPDH) primers were always included as a reference. PCR products were separated by electrophoresis in 1% agarose gel and visualized by staining with ethidium bromide.

The primers used in RT–PCR was followed:

GAPDH(forward): GGTCGGAGTCAACGGATTTGGTCG;
GAPDH(reverse): CCTCCGACGCCTGCTTCACCAC;
p27(forward): TTGCCCGAGTTCTACTACAGACCCC;
p27(reverse): CGAGCTGTTTACGTTTGACG;
BclxL(forward): ATGAACTCTTCCGGGATGG;
BclxL(reverse): TGGATCCAAGGCTCTAGGTG;
BIM(forward): TCCCTACAGACAGAGCCACAAGGT;
BIM(reverse): CAGGTTCAGCCTGCCTCATGGAAG;
GADD45(forward): ACGAGGACGACGACAGAGAT;
GADD45(reverse): GCAGGATCCTTCCATTGAGA.

The PCR program was: 10 min at 94°C, followed by 25 cycles (30 s at 94°C, 30 s at 54°C, 1 min at 72°C), followed by 7 min extension at 72°C.

Acknowledgements

We thank O Niwa and A Balmain for helpful comments on the paper. This work was supported by grants-in-aid for Cancer Research from the Ministries of Education, Science, Art and Sports, and of Health and Welfare of Japan.

References

Andegeko Y, Moyal L, Mittelman L, Tsarfaty I, Shiloh Y. (2001). Nuclear retention of ATM at sites of DNA double strand breaks. *J Biol Chem* **276**: 38224–38230.

Abraham RT. (2001). Cell-cycle checkpoint signaling through the ATM and ATR kinases. *Genes Dev* **15**: 2177–2196.

Alam A, Cohen LY, Aouad S, Sekaly RP. (1999). Early activation of caspases during T lymphocyte stimulation results in selective substrate cleavage in nonapoptotic cells. *J Exp Med* **190**: 1879–1890.

Avram D, Fields A, Pretty On Top K, Nevrivy DJ, Ishmael JE, Leid M. (2000). Isolation of a novel family of C2H2 zinc finger proteins implicated in transcriptional repression mediated by chicken ovalbumin upstream promoter transcription factor (COUP-TF) orphan nuclear receptors. *J Biol Chem* **275**: 10315–10322.

Bagheri-Yarmand R, Talukder AH, Wang RA, Vadlamudi RK, Kumar R. (2004). Metastasis-associated protein 1 deregulation causes inappropriate mammary gland development and tumorigenesis. *Development* **131**: 3469–3479.

Bartkova J, Horejsi Z, Koed K, Kramer A, Tort F, Zieger K *et al*. (2005). DNA damage response as a candidate anti-cancer barrier in early human tumorigenesis. *Nature* **434**: 864–870.

Brunet A, Sweeney LB, Sturgill JF, Chua KF, Greer PL, Lin Y *et al*. (2004). Stress-dependent regulation of FOXO transcription factors by the SIRT1 deacetylase. *Science* **303**: 2011–2015.

Chen Y, Sanchez Y. (2004). Chk1 in the DNA damage response: conserved roles from yeasts to mammals. *DNA Repair (Amst)* **3**: 1025–1032.

Cismasiu VB, Adamo K, Gecewicz J, Duque J, Lin Q, Avram D. (2005). BCL11B functionally associates with the NuRD complex in T lymphocytes to repress targeted promoter. *Oncogene* **24**: 6753–6764.

Clarke CA, Bennett LN, Clarke PR. (2005). Cleavage of Claspin by caspase-7 during apoptosis inhibits the Chk1 pathway. *J Biol Chem* **280**: 35337–35345.

Di Cristofano A, De Acetis M, Koff A, Cordon-Cardo C, Pandolfi PP. (2001). Pten and $p27^{KIP1}$ cooperate in prostate cancer tumor suppression in the mouse. *Nat Genet* **27**: 222–224.

Eguchi-Ishimae M, Eguchi M, Ishii E, Miyazaki S, Ueda K, Kamada N *et al*. (2001). Breakage and fusion of the TEL (ETV6) gene in immature B lymphocytes induced by apoptogenic signals. *Blood* **97**: 737–743.

Fero ML, Randel E, Gurley KE, Roberts JM, Kemp CJ. (1998). The murine gene $p27^{Kip1}$ is haplo-insufficient for tumor suppression. *Nature* **396**: 177–180.

Fero ML, Rivkin M, Tasch M, Porter P, Carow CE, Firpo E *et al*. (1996). A syndrome of multiorgan hyperplasia with

features of gigantism, tumorigenesis, and female sterility in p27(Kip1)-deficient mice. *Cell* **85**: 733–744.

Flatten K, Dai N, Vroman BT, Loegering D, Erlichman C, Karnitz LM *et al.* (2005). The role of checkpoint kinase 1 in sensitivity to topoisomerase I poisons. *J Biol Chem* **280**: 14349–14355.

Gorgoulis VG, Vassiliou LV, Karakaidos P, Zacharatos P, Kotsinas A, Liloglou T *et al.* (2005). Activation of the DNA damage checkpoint and genomic instability in human precancerous lesions. *Nature* **434**: 907–913.

Gounari F, Aifantis I, Khazaie K, Hoeflinger S, Harad N, Taketo MM *et al.* (2001). Somatic activation of β-catenin bypasses pre-TCR signaling and TCR selection in thymocyte development. *Nat Immunol* **2**: 863–969.

Hoeppner DJ, Hengartner MO, Schnabel R. (2001). Engulfment genes cooperate with ced-3 to promote cell death in *Caenorhabditis elegans*. *Nature* **412**: 202–206.

Inoue J, Kanefuji T, Okazuka K, Watanabe H, Mishima Y, Kominami R. (2006). Expression of TCR$\alpha\beta$ partly rescues developmental arrest and apoptosis of $\alpha\beta$T cells in Bcl11b$^{-/-}$ mice. *J Immunol* **176**: 5871–5879.

Kastan MB, Bartek J. (2004). Cell-cycle checkpoints and cancer. *Nature* **432**: 316–323.

Kiyokawa H, Kineman RD, Manova-Todorova KO, Soares VC, Hoffman ES, Ono M *et al.* (1996). Enhanced growth of mice lacking the cyclin-dependent kinase inhibitor function of p27(Kip1). *Cell* **85**: 721–732.

Lam MH, Liu Q, Elledge SJ, Rosen JM. (2004). Chk1 is haploinsufficient for multiple functions critical to tumor suppression. *Cancer Cell* **6**: 45–59.

Levine AJ, Feng Z, Mak TW, You H, Jin S. (2006). Coordination and communication between the p53 and IGF-1-AKT-TOR signal transduction pathways. *Genes Dev* **20**: 267–275.

Lin SY, Li K, Stewart GS, Elledge SJ. (2004). Human Claspin works with BRCA1 to both positively and negatively regulate cell proliferation. *Proc Natl Acad Sci USA* **101**: 6484–6489.

Liu Q, Guntuku S, Cui XS, Matsuoka S, Cortez D, Tamai K *et al.* (2000). Chk1 is an essential kinase that is regulated by Atr and required for the G(2)/M DNA damage checkpoint. *Genes Dev* **14**: 1448–1459.

Motoyama N, Wang F, Roth KA, Sawa H, Nakayama K, Nakayama K *et al.* (1995). Massive cell death of immature hematopoietic cells and neurons in Bcl-x-deficient mice. *Science* **267**: 1506–1510.

Motta MC, Divecha N, Lemieux M, Kamel C, Chen D, Gu W *et al.* (2004). Mammalian SIRT1 represses forkhead transcription factors. *Cell* **116**: 551–563.

Nagel S, Kaufmann M, Drexler HG, MacLeod RA. (2003). The cardiac homeobox gene NKX2-5 is deregulated by juxtaposition with BCL11B in pediatric T-ALL cell lines via a novel t(5;14)(q35.1q32.2). *Cancer Res* **63**: 5329–5334.

Nakayama K, Ishida N, Shirane M, Inomata A, Inoue T, Shishido N *et al.* (1996). Mice lacking p27(Kip1) display increased body size, multiple organ hyperplasia, retinal dysplasia, and pituitary tumors. *Cell* **85**: 707–720.

Nakayama K, Nagahama H, Minamishima YA, Miyake S, Ishida N, Hatakeyama S *et al.* (2004). Skp2-mediated degradation of p27 regulates progression into mitosis. *Dev Cell* **6**: 661–672.

Przybylski GK, Dik WA, Wanzeck J, Grabarczyk P, Majunke S, Martin-Subero JI *et al.* (2005). Disruption of the BCL11B gene through inv(14)(q11.2q32.31) results in the expression of BCL11B-TRDC fusion transcripts and is associated with the absence of wild-type BCL11B transcripts in T-ALL. *Leukemia* **19**: 201–208.

Reddien PW, Cameron S, Horvitz HR. (2001). Phagocytosis promotes programmed cell death in Celegans. *Nature* **412**: 198–202.

Sakata J, Inoue J, Ohi H, Kosugi-Okano H, Mishima Y, Hatakeyama K *et al.* (2004). Involvement of V(D)J recombinase in the generation of intragenic deletions in the Bcl11b/Bcl11b tumor suppressor gene in γ-ray-induced thymic lymphomas and in normal thymus of the mouse. *Carcinogenesis* **25**: 1069–1075.

Sanchez Y, Wong C, Thoma RS, Richman R, Wu Z, Piwnica-Worms H *et al.* (1997). Conservation of the Chk1 checkpoint pathway in mammals: linkage of DNA damage to Cdk regulation through Cdc25. *Science* **277**: 1497–1501.

Satterwhite E, Sonoki T, Willis TG, Harder L, Nowak R, Arriola EL *et al.* (2001). The BCL11 gene family: involvement of BCL11A in lymphoid malignancies. *Blood* **98**: 3413–3420.

Senawong T, Peterson VJ, Avram D, Shepherd DM, Frye RA, Minucci S *et al.* (2003). Involvement of the histone deacetylase SIRT1 in chicken ovalbumin upstream promoter transcription factor (COUP-TF)-interacting protein 2-mediated transcriptional repression. *J Biol Chem* **278**: 43041–43050.

Shinbo T, Matsuki A, Matsumoto Y, Kosugi S, Takahashi H, Niwa O *et al.* (1999). Allelic loss mapping and physical delineation of a region harboring a putative thymic lymphoma gene on chromosome 12. *Oncogene* **12**: 4131–4136.

Takai H, Tominaga K, Motoyama N, Minamishima YA, Nagahama H, Tsukiyama T *et al.* (2000). Aberrant cell-cycle checkpoint function and early embryonic death in Chk1(−/−) mice. *Genes Dev* **14**: 1439–1447.

van de Wetering M, de Lau W, Clevers H. (2002). WNT signaling and lymphocyte development. *Cell* **109**: S13–S19.

Wakabayashi Y, Inoue J, Takahashi Y, Matsuki A, Kosugi-Okano H, Shinbo T *et al.* (2003a). Homozygous deletions and point mutations of the Bcl11b/Bcl11b gene in γ-ray induced mouse thymic lymphomas. *Biochem Biophys Res Commun* **301**: 598–603.

Wakabayashi Y, Watanabe H, Inoue J, Takeda N, Sakata J, Mishima Y *et al.* (2003b). Bcl11b is required for differentiation and survival of$\alpha\beta$ T lymphocytes. *Nat Immunol* **4**: 533–539.

Walworth N, Davey S, Beach D. (1993). Fission yeast chk1 protein kinase links the rad checkpoint pathway to cdc2. *Nature* **363**: 368–371.

Zhao H, Watkins JL, Piwnica-Worms H. (2002). Disruption of the checkpoint kinase 1/cell division cycle 25A pathway abrogates ionizing radiation-induced S and G2 checkpoints. *Proc Natl Acad Sci USA* **99**: 14795–14800.

Zhou BB, Bartek J. (2004). Targeting the checkpoint kinases: chemosensitization versus chemoprotection. *Nat Rev Cancer* **4**: 216–225.

Zou L, Elledge SJ. (2003). Sensing DNA damage through ATRIP recognition of RPA-ssDNA complexes. *Science* **300**: 1542–1548.

Supplementary Information accompanies the paper on the Oncogene website (http://www.nature.com/onc).

Available online at www.sciencedirect.com
ScienceDirect
Life Sciences 80 (2007) 1335–1344
Life Sciences
www.elsevier.com/locate/lifescie

An inhibitor of c-*Jun* NH2-terminal kinase, SP600125, protects mice from D-galactosamine/lipopolysaccharide-induced hepatic failure by modulating BH3-only proteins

Masaaki Takamura [a,*], Yasunobu Matsuda [a], Satoshi Yamagiwa [a], Yasushi Tamura [a], Yutaka Honda [a], Kenji Suzuki [a], Takafumi Ichida [b], Yutaka Aoyagi [a]

[a] *Department of Gastroenterology and Hepatology, Niigata University Graduate School of Medical and Dental Sciences, 1-757 Asahimachi-dori, Niigata 951-8510, Japan*

[b] *Department of Gastroenterology, Juntendo University School of Medicine, Shizuoka Hospital, 1129 Nagaoka, Izunokuni, Shizuoka 410-2295, Japan*

Received 21 July 2006; accepted 21 December 2006

Abstract

Fulminant hepatic failure (FHF) is a dramatic clinical syndrome characterized by massive hepatocyte apoptosis and very high mortality. The c-*Jun*-N-terminal kinase (JNK) pathway is an important stress-responsive kinase activated by several forms of liver injury. The aim of this study is to assess the role of JNK during D-galactosamine (GalN)/lipopolysaccharide (LPS)-induced liver injury, an experimental model of FHF, using SP600125, a small molecule JNK-specific inhibitor. Mice were given an intraperitoneal dose of GalN (800 μg/g body weight)/LPS (100 ng/g body weight) with and without subcutaneous SP600125 (50 mg/kg body weight) treatment (at 6 and 2 h before and 2 h after GalN/LPS administration). GalN/LPS treatment induced sustained JNK activation. Administration of SP600125 diminished JNK activity, suppressed lethality and the elevation of both serum alanine aminotransferase and aspartate aminotransferase, but had no effect on serum tumor necrosis factor-α, and reduced hepatocyte apoptosis after GalN/LPS administration. In support of the role of JNK in promoting the mitochondria-mediated apoptosis pathway, SP600125 prevented cytochrome *c* release, caspase-9 and caspase-3 activity. Moreover, SP600125 downregulated the mRNA and protein expression of Bad in the early periods following GalN/LPS injection and prevented Bid cleavage in the late periods. These results confirm the role of JNK as a critical apoptotic mediator in GalN/LPS-induced FHF. SP600125 has the potential to protect FHF by downregulating Bad and inhibiting Bid cleavage.

Keywords: SP600125; JNK; Hepatic failure; Hepatocyte apoptosis; Cytochrome *c*; Bad; Bid

Introduction

Apoptosis, or programmed cell death, is essential to many biological processes in multicellular organisms, including embryonic development, immune responses, tissue homeostasis, and normal cell turnover (Thompson, 1995; Jacobson et al., 1997). Dysregulated apoptosis contributes to many pathogeneses, including tumor promotion, autoimmune and immunodeficiency diseases, neurodegenerative disorders, and fulminant hepatic failure (FHF) (Lee, 1993; Evan and Littlewood, 1998). FHF is a life-threatening illness, which is induced by viruses, alcohol or hepatotoxic drugs, and is marked by a massive degree of hepatocyte apoptosis. Mortality due to FHF remains high despite progress in medical therapy. Recently, liver transplantation has reduced mortality to some degree, but the chronic shortage of donor livers has limited its application. In fact, of 308 patients with FHF in the United States, 28% died while awaiting liver transplantation (Lee, 2003).

Abbreviations: FHF, fulminant hepatic failure; MAPK, mitogen-activated protein kinase; JNK, c-*Jun*-N-terminal kinase; GalN, D-galactosamine; LPS, lipopolysaccharide; TNF, tumor necrosis factor; I/R, ischemia/reperfusion; TBS, Tris-buffered saline; ALT, alanine aminotransferase; AST, aspartate aminotransferase; TUNEL, *in situ* terminal deoxynucleotidyl transferase-mediated dUTP nick-end labeling; PBS, phosphate-buffered saline; PCR, polymerase chain reaction.

* Corresponding author. Tel.: +81 25 227 2207; fax: +81 25 227 0776.
E-mail address: atmc@hotmail.co.jp (M. Takamura).

0024-3205/$ - see front matter © 2007 Elsevier Inc. All rights reserved.
doi:10.1016/j.lfs.2006.12.034

The mitogen-activated protein kinase (MAPK) family represents a group of proteins involved in the signal transduction of a variety of cellular stimuli. The c-*Jun* NH_2-terminal kinase (JNK) is a member of the MAPK family, and binds to the NH_2-terminal activation domain of c-*Jun* and phosphorylates c-*Jun* on Ser-63 and -73, causing increased transcriptional activity (Pulverer et al., 1991; Adler et al., 1992). JNK activation is known to trigger apoptosis in response to environmental stresses as well as inflammatory cytokines such as tumor necrosis factor (TNF)-α (Ip and Davis, 1998). The JNK signaling pathway is activated in various forms of liver injury (Trautwein et al., 1998; Bendinelli et al., 1996; Bradham et al., 1997; Schattenberg et al., 2006; Chang et al., 2006). Recently, several studies, based on the gene-knockout approach, have convincingly demonstrated the critical role of JNK in hepatocyte apoptosis, which was induced by concanavalin A, a methionine- and choline-deficient diet, or D-galactosamine (GalN)/lipopolysaccharide (LPS) (Schattenberg et al., 2006; Chang et al., 2006; Maeda et al., 2003; Wang et al., 2006). The recent development of JNK-specific inhibitors has greatly accelerated our understanding of this signaling pathway in hepatocyte apoptosis. One such inhibitor is an anthrapyrazolone inhibitor of JNK, SP600125, which shows 300-fold selective inhibition of JNK over extracellularly regulated kinases and p38 MAPKs, the closest kinase relatives of JNK (Bennett et al., 2001). Another class of newly developed JNK-specific inhibitors is peptide-based, such as a 20-amino-acid peptide derived from the JNK binding domain of JNK-interacting protein-1 (Bonny et al., 2001), which has recently been tested successfully in a model of FHF (Chang et al., 2006).

In this study, we first confirmed whether JNK activation was critical for GalN/LPS-induced hepatocyte apoptosis in vivo. We used SP600125 to show that liver injury is causatively coupled to JNK activation. Next, we investigated the mechanism of JNK in apoptosis signaling in the liver of GalN/LPS-treated mice.

Material and methods

Antibodies

Anti-phospho-JNK (#9251), anti-JNK (#9252), anti-phospho-c-*Jun* (#9261), anti-c-*Jun* (#9162), anti-Bad (#9292), anti-Bax (#2772) antibodies were purchased from Cell Signaling Technology (Beverly, MA). Anti-Bim/BOD (AAP-330) antibody was purchased from Stressgen (Victoria, BC). Anti-cytochrome *c* (clone 7H8.2C12), anti-Bcl-XL (clone 44), and anti-Bcl-2 (clone 7) antibodies were purchased from BD Biosciences Pharmingen (San Diego, CA). Anti-Bid (MAB860) and anti-β-actin (clone AC-15) antibodies were purchased from R and D systems (Minneapolis, MN) and Sigma (St. Louis, MO), respectively.

Animals and experimental protocols

Six-week-old male BALB/c mice (CLEA, Shizuoka, Japan) were maintained at the Animal Center of Niigata University School of Medicine under specific pathogen-free conditions. The in vivo experiments were performed according to the Niigata University School of Medicine Guidelines for the Care and Use of Laboratory Animals. For the preparation of mice with GalN/LPS-induced FHF, mice were given an intraperitoneal injection of GalN (800 μg/g body weight; Sigma), followed immediately by an intraperitoneal injection of LPS (100 ng/g body weight; Sigma). The mice were subcutaneously injected three times with SP600125 (50 mg/kg body weight; BIOMOL, Plymouth, PA) in PPCES vehicle (30% PEG–400/20% polypropylene glycol/15% Cremophor EL/5% ethanol/30% saline) at 6 and 2 h before and 2 h after GalN/LPS administration. Control mice were administered the GalN/LPS and then injected three times with PPCES vehicle alone. Serum and liver samples were obtained at 0, 2, 4, 6, 8, and 24 h after GalN/LPS administration ($n=5$ for each group).

Western blot analysis

Snap-frozen liver samples were lysed using ice-cold lysis buffer (50 mM Tris–HCl (pH 8.0), 150 mM NaCl, 0.1% SDS, 1% Nonidet P-40, 1 mM Na_3VO_4, 50 mM NaF). Twenty to fifty μg of proteins were resolved on 10–15% sodium dodecyl sulfate polyacrylamide gels and transferred to Immobilon membranes (Millipore, Bedford, MA). After blocking, the filters were reacted with primary antibodies followed by horseradish peroxidase-conjugated secondary antibodies. Peroxidase-labeled bands were visualized with an ECL detection system (Amersham Biosciences, Buckinghamshire, UK). For confirmation of equal loading, the blots were reprobed with anti-β-actin antibody. Quantitative analysis of bands was performed using the NIH Image software package (version 1.63).

Immunohistochemistry

Sections (4 μm thick) of formalin-fixed, paraffin-embedded tissues were deparaffinized with a xylene and ethanol series, and then stained with anti-phospho-c-*Jun* and anti-cytochrome *c* antibodies. Bound primary antibody was visualized by using a polymer-labeled enhancement system (Envision+System, Peroxidase; DakoCytomation).

Analysis of alanine aminotransferase, aspartate aminotransferase and TNF-α levels

Serum levels of liver enzymes, including alanine aminotransferase (ALT) and aspartate aminotransferase (AST), were determined using an automatic analyzer (SRL, Tokyo, Japan). Serum TNF-α (Mouse TNF-α mouse ELISA kit; Pierce Endogen, Rockford, IL) was determined by enzyme-linked immunosorbent assay according to the manufacturer's instructions.

Liver histology and terminal deoxynucleotidyl transferase-mediated dUTP nick-end labeling

The formalin-fixed livers were paraffin-embedded, and liver sections were stained with hematoxylin-eosin. Apoptotic hepatocytes were detected using the in situ terminal deoxynucleotidyl

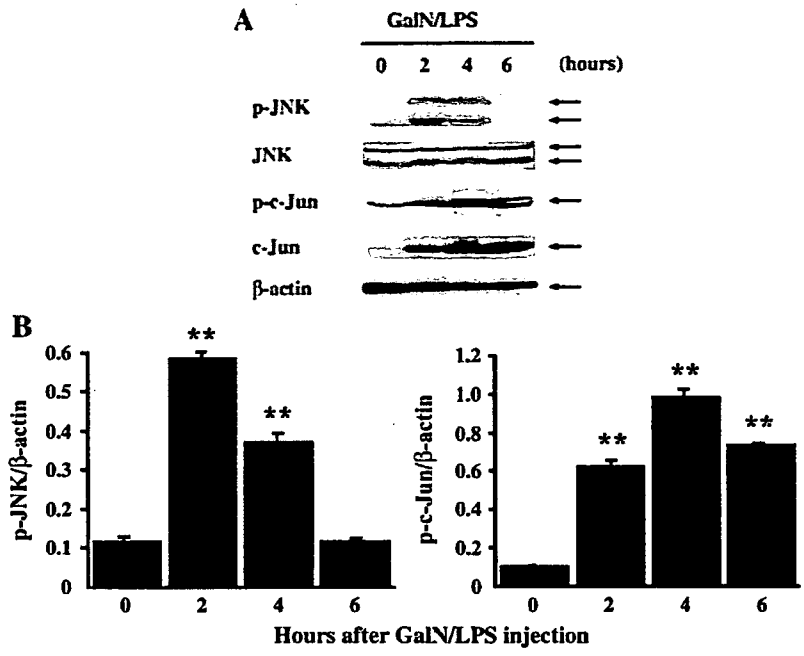

Fig. 1. (A) The profile of JNK activation in the livers of GalN/LPS-treated mice. Equal protein loading was confirmed using β-actin as a reference standard. (B) The graphs show relative values for levels of p-JNK or p-c-*Jun* normalized to β-actin after GalN/LPS administration. Data from three independent experiments are averaged and are represented as the means±SD. $^{**}P<0.01$, vs 0 h.

transferase-mediated dUTP nick-end labeling (TUNEL) method with a commercial kit (Takara, Tokyo, Japan) according to the manufacturer's protocol. Tissue sections were observed by fluorescence microscopy using a microscope (Axio Imager A1; Carl Zeiss MicroImaging, Inc.). Images were acquired using a digital camera (Axiocam MRc5; Carl Zeiss MicroImaging, Inc.) and Axiovision software (Carl Zeiss MicroImaging, Inc.) and then processed with the Photoshop software package (Adobe). As a negative control, PBS was substituted for the mixture of labeling safe buffer and terminal deoxynucleotidyl transferase.

DNA fragmentation assay

Chromosomal DNA was extracted from liver tissues using the DNeasy Tissue Kit (Qiagen, Maryland, USA) in accordance with the manufacturer s protocol. Two μg of each DNA was loaded onto 1.8% agarose gel containing ethidium bromide, electrophoresed in Tris acetate/EDTA buffer for 30 min at 100 V, and photographed under ultraviolet illumination.

Caspase-3 and -9 activities

Caspase-3 and -9 activities in liver tissues were measured using Caspase-3 and -9 Colorimetric Assay Kits (MBL, Nagoya, Japan), respectively, according to the manufacturer's instructions. Briefly, liver tissues were homogenized in cell lysis buffer included in the kit. The homogenates were centrifuged for 15 min at 15,000 rpm at 4 °C, and the supernatant (100 μg of proteins) was incubated with DEVD-*p*NA, LEHD-*p*NA substrates for caspase-3, and -9, respectively, in reaction buffer for 2 h at 37 °C. Absorbance was measured at 405 nm.

Reverse-transcriptase polymerase chain reaction

Total RNA was isolated using the RNeasy Mini kit (Qiagen) according to the manufacturer's protocol. cDNA was synthesized from 1 μg of total RNA with an oligo(dT)$_{18}$ primer using a Transcriptor First Strand cDNA Synthesis Kit (Roche, Penzberg, Germany). Next, the reverse transcriptase product was amplified with Takara Taq (Takara, Shiga, Japan). The primers used in this experiment were as follows: 5′-GGAAGACGC-TAGTGCTACAGA-3′, 5′-GACCTCCTTTGCCCAAGTTT-3′ for mouse Bad; 5′-GTATGTCGTGGAGTCTACTGGTGT-3′, 5′-TACTCCTTGGAGGCCATGTAGGCC-3′ for GAPDH. These polymerase chain reaction (PCR) primers were purchased from Japan Bio Services (Saitama, Japan). The PCR amplification was carried out in 30 cycles of denaturation (94 °C, 1 min), annealing (60 °C, 1 min), elongation (72 °C, 1 min) and with an additional 10 min of final extension at 72 °C. The PCR product was analyzed by running on 1.5% agarose gel.

Statistical analysis

Data are expressed as the means±SD. Student's *t* test was used for comparisons between 2 groups and differences at $P<0.05$ were considered significant. Kaplan–Meier survival analysis was used for survival data by log-rank test.

Results

Activation of JNK in the liver of GalN/LPS-treated mice

To confirm that JNK activation occurred in the liver of GalN/LPS-treated mice, we examined phosphorylation of JNK and

c-*Jun*, a major downstream target of JNK, by Western blot analysis (Fig. 1A). An increase of immunoreactivity was seen at 2 h after GalN/LPS administration for phosphorylated (p-) JNK, p-c-*Jun* and c-*Jun*. However, p-JNK immunoreactivity was not seen at 6 h, whereas p-c-*Jun* and c-*Jun* immunoreactivity remained markedly elevated by this time. Densitometric analysis revealed that the relative level of p-JNK normalized to that of β-actin was significantly enhanced beginning at 2 h after GalN/LPS administration, returning to the baseline level by 6 h, whereas that of p-c-*Jun* normalized to β-actin remained significantly elevated at 6 h (Fig. 1B).

Inhibition of JNK activity by SP600125 in the liver of GalN/LPS-treated mice

To test whether it was possible to modulate JNK activity in the liver of GalN/LPS-treated mice, a specific JNK inhibitor, SP600125 (50 mg/kg body weight), or vehicle (without SP600125) was administered 6 and 2 h before and 2 h after GalN/LPS administration. Western blot and densitometric analyses revealed that p-c-*Jun* levels were significantly attenuated at 2 (at the last administration of SP600125), 4, and 6 h after GalN/LPS administration by SP600125, whereas c-*Jun* levels were significantly attenuated at 6 h only after GalN/LPS administration by SP600125 (Fig. 2A and B). Similarly, immunohistochemistry showed that p-c-*Jun* expression was markedly decreased in the livers of SP600125-treated mice 4 h after GalN/LPS administration, compared with vehicle-treated mice (Fig. 2C). Additional studies showed that SP600125 did not affect other signaling pathways such as phosphorylation of ATF2 or degradation of IκB-α (data not shown). These findings suggest that SP600125 is specific and effective in blocking JNK activity in the liver of GalN/LPS-treated mice.

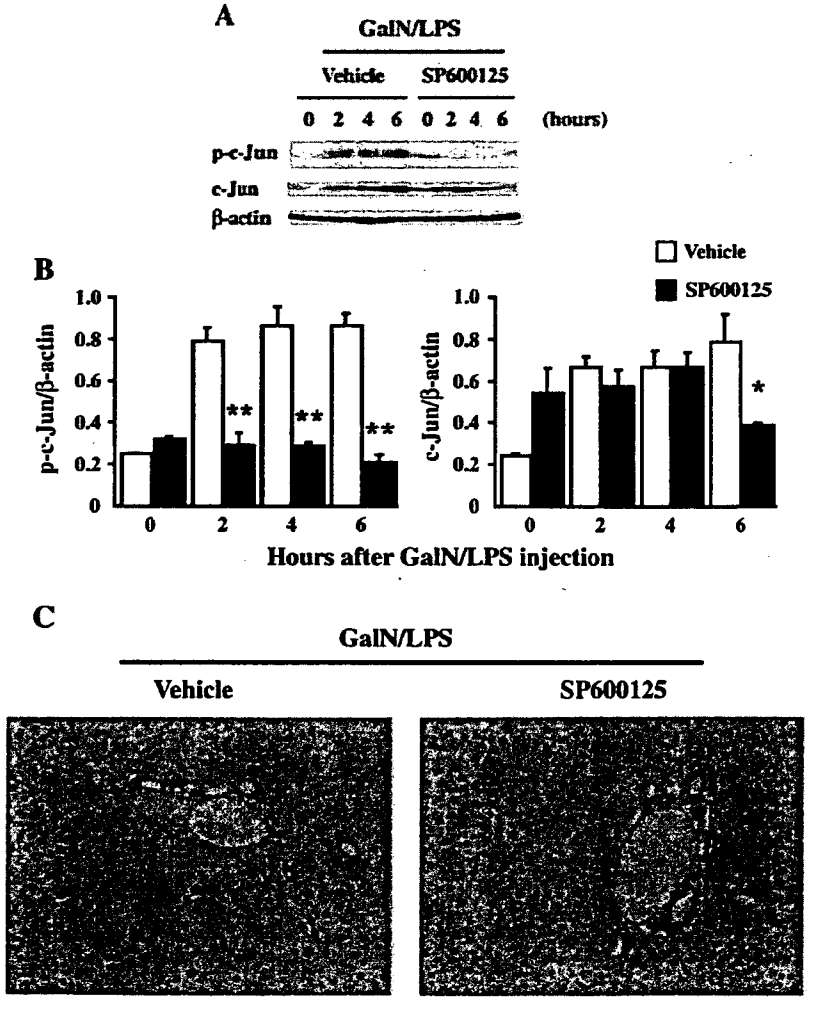

Fig. 2. Effect of SP600125 on JNK activation in the livers of GalN/LPS-treated mice. (A) Western blot analysis of p-c-*Jun* or c-*Jun* in the livers of SP600125-treated mice and vehicle-treated mice after GalN/LPS administration. Equal protein loading was confirmed using β-actin as a reference standard. (B) The graphs show relative values for levels of p-c-*Jun* or c-*Jun* normalized to β-actin after GalN/LPS administration. Data from three independent experiments are averaged and are represented as the means±SD. $^{*}P<0.05$, $^{**}P<0.01$, vs vehicle-treated mice. (C) Immunohistochemistry for p-c-*Jun* in the livers of SP600125-treated mice and vehicle-treated mice at 4 h after GalN/LPS administration.

Suppression by SP600125 of lethality in mice with GalN/LPS-induced FHF

To assess the beneficial effect of JNK inhibition on lethality in mice with GalN/LPS-induced FHF, survival studies were performed. The survival rate of vehicle-treated mice was only 14% (1 of 7) at 24 h after GalN/LPS administration. In sharp contrast, the survival rate of SP600125-treated mice was improved to 80% (4 of 5) at 24 h after GalN/LPS administration ($P<0.05$; Fig. 3).

The changes in serum ALT (vehicle-treated mice, 1935±1274 IU/L; SP600125-treated mice, 262±59 IU/L) and AST (vehicle-treated mice, 1229±486 IU/L; SP600125-treated mice, 485±38 IU/L) levels by GalN/LPS administration were more marked in vehicle-treated mice than in SP600125-treated mice ($P<0.05$ for each; Fig. 4A).

It has been reported previously that the serum TNF-α level increases rapidly and markedly in GalN/LPS-treated mice, reaching a maximal value within 1 to 2 h after GalN/LPS administration (Chang et al., 2006; Wang et al., 2006; Nakama et al., 2001). To clarify whether SP600125 exerts its effect by blocking TNF-α production, we measured the serum TNF-α level 2 h after GalN/LPS administration. We observed that SP600125 treatment did not suppress the serum TNF-α level (vehicle-treated mice, 2657±1420 pg/mL; SP600125-treated mice, 2480±284 pg/mL) in GalN/LPS-treated mice (Fig. 4B).

Reduction of hepatocyte apoptosis by SP600125 in mice with GalN/LPS-induced FHF

To confirm the preventive effects of SP600125 against liver injury, we assessed the liver architecture histopathologically after GalN/LPS administration. Apoptotic hepatocytes with intralobular hemorrhage were observed, beginning 6 h after GalN/LPS administration (data not shown). At 8 h after GalN/LPS administration, severe liver damage, including numerous apoptotic hepatocytes and massive necrosis with intralobular hemorrhage, was observed in the livers of vehicle-treated mice, whereas this was hardly observed in the livers of SP600125-treated mice (Fig. 5A).

To obtain further evidence that SP600125 prevents hepatocyte apoptosis, apoptotic hepatocytes were detected by TUNEL staining. A large number of TUNEL-positive hepatocytes were

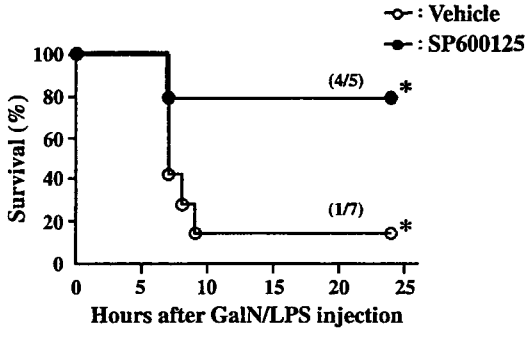

Fig. 3. Effect of SP600125 on the survival curve of GalN/LPS-treated mice. *$P<0.05$, vs vehicle-treated mice.

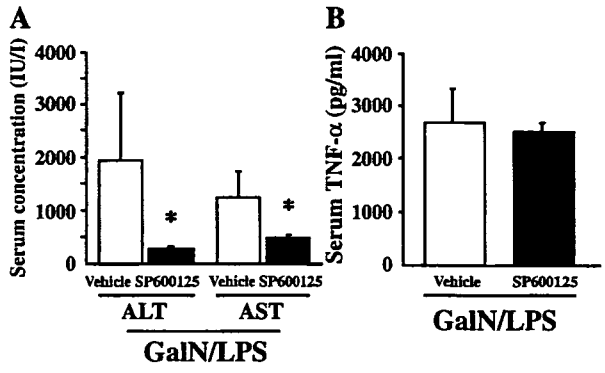

Fig. 4. (A) Effect of SP600125 on serum ALT and AST levels of mice at 6 h after GalN/LPS administration. (B) Effect of SP600125 on serum TNF-α levels of mice at 2 h after GalN/LPS administration. Each value represents the means± SD for 5 mice. *$P<0.05$, vs vehicle-treated mice.

seen in the livers of vehicle-treated mice 8 h after GalN/LPS administration; however, only a few TUNEL-positive hepatocytes were present in the livers of SP600125-treated mice even 8 h after GalN/LPS administration (Fig. 5B).

Consistent with these histopathological observations and the TUNEL assay, DNA fragmentation was detected in the livers of vehicle-treated mice 6 h after GalN/LPS administration, whereas this was not detected in the livers of SP600125-treated mice (Fig. 5C).

Attenuation of the mitochondria-mediated apoptosis pathway by SP600125 in mice with GalN/LPS-induced FHF

Not only the death receptor-mediated (TNF/Fas ligand-mediated) apoptosis pathway but also the mitochondria-mediated apoptosis pathway plays a critical role in hepatocyte apoptosis. In this study, we examined whether JNK activity contributed to mitochondrial damage and to activation of the downstream apoptosis cascade after GalN/LPS administration. First, the release of cytochrome *c* into the cytosolic fraction, an indicator of compromised mitochondrial integrity, was assessed using immunohistochemistry. In untreated livers, cytochrome *c* appeared in the cytoplasm as a punctate (mitochondrial) staining pattern (data not shown). Six h after administration, cytochrome *c* in the hepatocytes appeared as a diffuse (cytosolic) staining pattern, whereas the punctate staining pattern was still prominent in the hepatocytes of SP600125-treated livers at 6 h after GalN/LPS administration (Fig. 6A). In line with its demonstrated inhibitory effect on the mitochondria-mediated apoptosis pathway, SP600125 diminished the activation of both caspase-9 and caspase-3 after GalN/LPS administration (Fig. 6B and C). These results suggest that JNK activity is required for the mitochondrial damage-mediated activation of cell death effectors, including caspase-9 and caspase-3.

Downregulation of bad expression and inhibition of bid cleavage by SP600125 in the livers of GalN/LPS-treated mice

Bcl-2 family proteins serve as critical regulators of the mitochondria-mediated apoptosis pathway, functioning as either

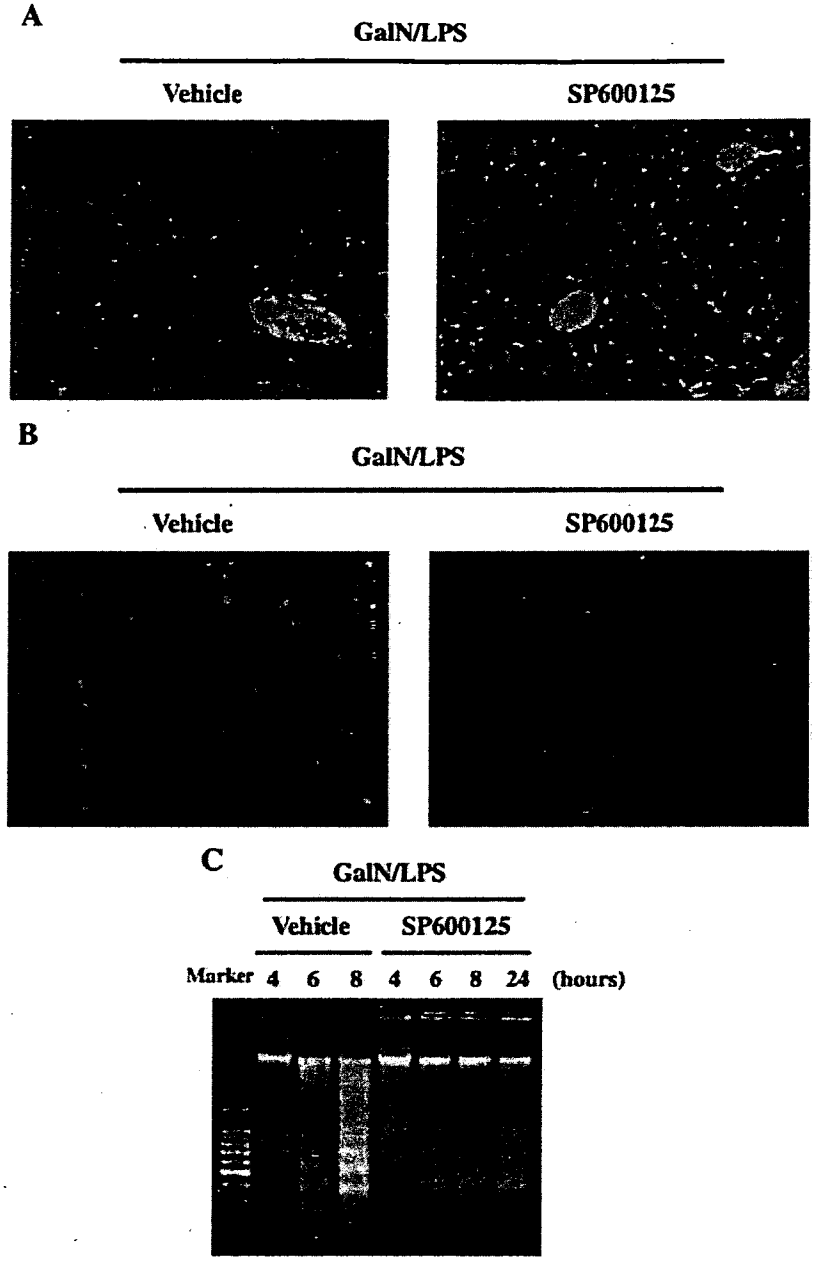

Fig. 5. (A) Histological examination of the liver in mice at 8 h after GalN/LPS administration with or without SP600125 (hematoxylin-eosin, ×100). (B) Detection of apoptotic hepatocytes in the liver of mice at 8 h after GalN/LPS administration with or without SP600125 (TUNEL, ×100). (C) DNA fragmentation in the livers of mice after GalN/LPS administration with or without SP600125.

inhibitors (e.g., Bcl-2, Bcl-XL, Bcl-w and Mcl-1) or promoters (e.g., Bax, Bid, Bad and Bim) of cell death (Gross et al., 1999). JNK modulates some Bcl-2 family proteins on multiple levels: transcriptional, post-transcriptional, and post-translational (Yamamoto et al., 1999; Putcha et al., 2001; Yu et al., 2004). We therefore examined Bcl-2 family protein expression by Western blot analysis in the livers of SP600125- and vehicle-treated mice after GalN/LPS administration (Fig. 7A). Among prosurvival members of the Bcl-2 family, there was no detectable expression of Bcl-2 protein in the livers of both vehicle- and SP600125-treated mice after GalN/LPS administration, and no differences in the protein level of Bcl-XL in the livers between vehicle- and SP600125-treated mice after GalN/LPS administration. On the other hand, among proapoptotic members of the Bcl-2 family, there were no differences in the protein level of Bim and Bax in the livers between vehicle- and SP600125-treated mice after GalN/LPS administration. Bid cleavage started in the livers of vehicle-treated mice 6 h after GalN/LPS administration, and SP600125 blocked Bid cleavage, as observed in other in vivo models (Uehara et al., 2005). Interestingly, there was no change in the protein level of Bad in the livers of vehicle-treated mice after GalN/LPS administration. However, the protein level was downregulated in the livers of SP600125-treated mice beginning at 2 h after GalN/LPS